FORMATION DAMAGE EVALUATION OF VISCOELASTIC-BASED STIMULATION FLUIDS

A Dissertation

by

SALAR AFRA

Submitted to the Office of Graduate and Professional Studies of
Texas A&M University
in partial fulfillment of the requirements for the degree of

DOCTOR OF PHILOSOPHY

Chair of Committee,	Hadi Nasrabadi
Committee Members,	Jerome Schubert
	Mahmoud El-Halwagi
	Maria A. Barrufet
Head of Department,	Jeff Spath

December 2020

Major Subject: Petroleum Engineering

ABSTRACT

Viscoelastic surfactants (VES) have been successfully applied in well stimulation treatments, including acid-diversion and hydraulic fracturing. However, high temperature, interactions of VES with metallic cations, alcohol-based additives, and nano-materials all interfere with the apparent viscosity of the VES-based fluids and reduce the efficiency of these systems and even lead to further damaging the formation. The main purpose of the present thesis is to characterize any possible interaction/reaction of typical VES-based solutions in the oil and gas industry with common acid and fracturing fluids additives and contaminations such as corrosion inhibitors, metal cations, and nano-materials.

Dynamic and static rheological properties of different VES-based acid systems were investigated to study the effects of additives on the viscoelasticity and surface tension of the VES system. Small angle X-ray Scattering was carried out to determine the morphology of the micellar structures in the VES-based systems. Infrared spectroscopy, UV-vis spectroscopy, and single X-ray crystallography were utilized to characterize the molecular interactions/reactions that lead to alteration of the macroscopic behavior of surfactant systems.

Formation of wormlike micelles in a system containing a zwitterionic C_{22}-tailed sulfobetaine surfactant in the presence of Fe^{3+} in HCl was demonstrated by rheological and SAXS profiles. The transition from viscoelastic behavior to non-Maxwellian elastic gel-like behavior after the addition of Fe^{3+} is confirmed through dynamic rheological measurements. The addition of different types of corrosion inhibitors to the VES solutions led to changes in the conformation of micellar structures and rheology of the VES-based

solutions. The addition of trace amounts of carbon nanotube (CNT), 0.04 to 0.2 wt%, to the VES solutions enhanced the rheological behavior of tested VES systems by approximately 40%. The main interactions/reactions are characterized to be acid-base reactions and hydrogen bonding. The results of this study also show that the amide part of VES is the leading functional group that can react/ interact with corrosion-inhibitor, CNT, and metal cations, screening the repulsion forces between surfactants headgroups and, as a result altering micellar structures.

The results of the present study can be used to design more efficient VES-based acid systems and prevent the occurrence of post-formation damage following the treatment.

DEDICATION

I dedicate this thesis to my parents, sister, brother, sister in law, and the late Dr. Hisham Nasr-El-Din for their continuous inspiration, support, and encouragement.

ACKNOWLEDGEMENTS

I express my deepest gratitude and appreciation to my former committee chair, the late Dr. Hisham A. Nasr-El-Din, for his continuous encouragement, guidance, and support throughout this research. I would like to truly appreciate Dr. Hadi Nasrabadi for agreeing to be my committee chair and for his huge support in such a tough situation. I would like to extend my appreciation to Dr. Maria A. Barrufet, Dr. Mahmoud El-Halwagi, and Dr. Jerome Schubert for serving as committee members.

Thanks also go to all of my friends and colleagues in my research group and the department faculty and staff for making my time at Texas A&M University a great experience. I would like to acknowledge all the supports from Dr. Jeff Spath to help my colleagues and me to successfully finalize our journeys at Texas A&M despite the tragic loss of Dr. Nasr-El-Din.

Last but not least, I thank my family for their encouragement, patience, and love.

CONTRIBUTORS AND FUNDING SOURCES

Contributors

This work was supported by a dissertation committee consisting of Professor Hadi Nasrabadi of the Department of Petroleum Engineering as chair and Professor Hisham Nasr-El-Din of the Department of Petroleum Engineering as a former chair. Professor Maria Barrufet, Professor Jerome Schubert of the Department of Petroleum Engineering, and Professor Mahmoud El-Halwagi of the Department of Chemical Engineering also served as members of my dissertation committee. All work for the dissertation was completed independently by the student.

Funding Soruces

Graduate study was supported by departmental funding.

NOMENCLATURE

a_0	Effective Area per Molecule
l_c	Maximum Effective Length
q	Magnitude of the Scattering Vector
A_{min}	Gibbs Molecular Area
C	Concentration
CMC	Critical Micelle Concentration
CNT	Carbon Nanotubes
DCl	Deuterated Hydrochloric Acid
DMF	N,N-dimethylformamide
DMSO	Dimethyl Sulfoxide
D_2O	Deuterated Oxide
EDAS	3-(N-erucamidopropyl-N,N-dimethyl ammonium) propane sulfonate
G′	Elastic Modulus
G″	Viscous Modulus
G_0	Elastic Modulus at Infinite Frequency
HCl	Hydrochloric Acid
I	Intensity Profile
IR	Infrared
NMR	Nuclear Magnetic Resonance
N_A	Avogadro's Number

P	Packing Parameter
R	Gas Constant
SMA	3-sulfopropyldimethyl-3-methacryl-amidopropylammonium
T	Temperature
T_k	Krafft Temperature
UV-Vis	Ultraviolet-visible
VES	Viscoelastic Surfactant
θ	Half of the Scattering Angle
γ	Surface Tension
λ	Wavelength
τ_b	Micelles Breaking Time
τ_{rep}	Micelles Reptation Time
v	Volume of the Lipophilic Chain
ω	Frequency
ω_c	Crossover Frequency
Γ_{CMC}	Surface Excess Concentration at CMC

TABLE OF CONTENTS

Page

LIST OF FIGURES

Page

LIST OF TABLES

Page

CHAPTER I

INTRODUCTION*

Viscoelastic Surfactant (VES)

Surfactant micelles are known for their self-assembled structure and flow behaviors and a subclass of these micelles that have significant applied and fundamental scientific interests as drug carriers, templates, and rheology modifiers [1,2]. Typically, with diameters of 2-5 nm and various lengths up to the micrometers, wormlike micelles exhibit rheological behaviors similar to polymer solutions [3]. Certain mixed surfactant solutions can enhance the rheological behaviors of these wormlike micelles, such as viscoelasticity, thermal stability, and shear thinning [4,5]. Wormlike micelles promote a more optimal alternative to polymers as their constant breaking and reforming at thermal equilibrium helps prevent mechanical degradation of the worms, making them very desirable as fracturing liquids [2,6,7].

Viscoelastic surfactants (VES) have been applied widely in the oil and gas industry because of their characteristic features, including rheology [8], drag-reducing ability [9,10], and easy clean-up [11] that make them interesting substitutes for polymers. VES applications can be advantageous in a wide variety of drilling, completion, and stimulation processes and formulations such as fracturing fluids [12,13], acid diverters

* Reprinted with permission from "Micellar growth and network formation in acidic solutions of a sulfobetaine zwitterionic surfactant triggered by an inorganic salt" by Afra, S. et al. 2020. Soft Matter, 16, 4494-4501, Copyright 2020 by Royal Society of Chemistry.

[14], and gravel-packing carrier fluids [15]. Difficulties associated with the application of polymer-based systems, such as controlling cross-linking, breaking in the narrow pH range, and maintaining the stability of polymers at high temperatures were also addressed in VES-based systems [16,17].

Rheological Behavior of VES-Based Systems

The main cause of the attractive rheological behavior of VES systems under certain conditions is the formation of specific colloidal structures based on noncovalent bonding called "wormlike micelles." The micellization occurs at a certain concentration, the critical micelle concentration (CMC), that can be affected by several physicochemical factors including temperature [18], ionic strength [19,20], pH [21,22], as well as surfactant properties, e.g., hydrophobe chain length [23], and its charge [24]. The structures of micelles in a solution can be predicted through the packing parameter concept:

$$P = \frac{v}{a_0 l_c} \tag{1}$$

where v is the volume of the lipophilic chain having a maximum effective length (l_c), and a_0 is the effective area per molecule at the surfactant-water interface. When the value of P is between 1/3 and 1/2, wormlike micelles are supposed to generate [25].

From the rheological point of view, the presence of wormlike micelles in a solution has been generally confirmed by the applicability of the Maxwellian model to that system. Rheologically, if the wormlike micelles behave like a fast-breaking system,

τ_b (breaking time) << τ_{rep} (reptation time), storage modulus (G′), and loss modulus (G″) can be described by Maxwellian equations as follow [4,26–30]:

$$G'(\omega) = \frac{\omega^2 \tau_R^2}{1 + \omega^2 \tau_R^2} G_0 \quad (2)$$

$$G''(\omega) = \frac{\omega \tau_R}{1 + \omega^2 \tau_R^2} G_0 \quad (3)$$

These equations imply that at low shear frequencies ($\omega < \omega_c$) G′ increases with ω by order of two, and G″ increases with ω linearly. Also, there is a maximum value for G″ at ω_c. Recent studies on wormlike micelles, especially those generated by surfactants with long alkyl chains, show the gel-like behavior of these systems, with G′ exceeding G″ at all frequency range with infinite relaxation time [20,31–34]. Because these systems resemble gel-like material formed by polymers, they are called living or dynamic polymers [35].

VES Applications in the Oil and Gas Industry

In the case of matrix acidizing, the notable rheological properties of wormlike micelles, as well as their recovery capacity (due to their dynamic behaviors), make them interesting substances as diversion agents. The surfactant-based acid systems have a low initial viscosity that can meet the minimum injectivity requirements while they reach the target zone their viscosity increases. Various parameters cause the viscosity improvement, i.e., higher temperature of the target reservoir [6,36,37], pH alteration of the system due to acid spending process [38–41], and production of Ca^{2+} and Mg^{2+} ions following by the

carbonate dissolution [8]. Moreover, difficulties associated with the application of polymer-based acid systems, e.g., controlling cross-linking and breaking in the narrow pH range and stability of polymers at high temperatures were addressed in VES-based diverting systems [17].

In many reservoirs, there is a layer of oil that can be trapped in the pores of oil-bearing rocks, causes an increase in production cost; because of this, finding new methods to extract the tertiary level of oil has been more desirable and lucrative. This level of oil recovery paves new lines of productivity in the petroleum industry, including hydraulic fracturing. Fracturing fluids offer an optimal technique to enhance the production of oil and gas in low-permeability reservoirs [42,43]. Maintaining a low cost, reducing formation damage, lowering concentration and molecular weight are just some of the approaches that can be taken to optimize these fluids [44,45]. Viscoelastic surfactants were introduced to apply in hydraulic fracturing fluids as a proppant carrier to replace polymers that possess high potential for formation damage. Yet, VES technology is limited by its low thermal stability and high leak-off behavior in high permeability formations. Nanomaterials are often used as additives since they can optimize fluid properties. However, these nanomaterials, like nanoparticles, are still imperfect, being expensive while increasing the molecular weight of the VES fluids [13].

Additives and Contaminations in the Oil and Gas Industry

Carbon Nanotubes

Multiwalled carbon nanotubes (CNT) offer a new and novel route for research in material and petroleum chemistry. In contrast to traditional nanoparticles, CNTs are strong

and flexible, which brings interesting applications as additives for rheological improvement [46,47]. Furthermore, the functionalization of CNTs allows for research flexibility for studying bonding. Despite the interesting properties of VES-CNT systems, not much research has been conducted on the rheological behaviors of zwitterionic, anionic, and nonionic VES fluid with multi functionalized CNT additive [1].

Ferric and Ferrous

Iron, both ferric and ferrous, are among the most prevalent, while most problematic components in the oilfield chemistry with an occurrence concentration of 200 to 100000 mg/L [48–50]. Ferric precipitation that begins at a pH of 1 and completes at pH of 2 has been noted as one the source of formation damage in acidizing treatments [51]. Moreover, sludge generation induced by ferric in the presence of hydrochloric acid is another source of formation damage, especially in the crude oils with unstable asphaltenes contents [52,53]. Several unsuccessful VES-based acid treatments have been reported that their results indicate the occurrence of formation damage after applying the treatment.

Corrosion Inhibitors

Because of the corrosivity of acids used in stimulation treatments, the application of corrosion inhibitors is inevitable to maintain the integrity of the tubular and production facilities. Corrosion inhibitors are mainly organic materials that are used in small amounts to control the corrosion rate of the exposed metallic compounds [54]. One of the main challenges regarding the application of corrosion inhibitors is their selective effectiveness with particular metallic materials and environments. Hence, there is a wide range of

corrosion inhibitors in the industry that should be investigated based on the applied acid, tubular materials, and temperature [55]. Nitrogen-containing heterocycles [56,57], acetylenic alcohols, aromatic aldehydes, alkenylphenones [58,59], and condensation products of amines and carbonyls [60–62] are among the chemical compounds used in the oil and gas industry as corrosion inhibitors.

Thiourea-based inhibitors and the quaternary ammonium compounds are among the most prevalent corrosion-inhibitor formulations in the oil and gas industry. To improve the effectiveness of these compounds in terms of isolating the metal surface and retarding its dissolution by the formation of a polymer-like film, different additives such as formic acid, acetic acid, and fatty acids are added to the corrosion inhibitor packages [63]. Also, other solvents have been used to facilitate handling by reducing viscosity and to ensure stability at various conditions. Moreover, solubility and dispersibility of corrosion inhibitors in the acid, as well as wettability of the acid-steel interface, would be enhanced in the presence of solvents [54].

VES compatibility with corrosion inhibitors, as well as other additives such as iron-control agents and H_2S scavengers, is an important issue in designing stimulation fluids. While some studies in the literature show no or slight effects of corrosion inhibitors on VES viscosity [13,64–66], several studies reported the adverse effects of additives, specifically corrosion inhibitors, on the performance of VES-based systems [67]. Nasr-El-Din et al. 2008 evaluated the effects of two industrial corrosion inhibitors, with aromatic ketone amine derivative and quaternary amine as active agents, on the viscosity of an amphoteric VES at live and spent conditions and showed the impairment of VES-based acid viscosity even at low concentrations (0.6 wt%) of corrosion inhibitors [68].

Hanafy et al. 2019 tested two corrosion inhibitors in the oil and gas industry with cationic and zwitterionic VESs and concluded that there is no reaction between corrosion inhibitors and VESs; however, the electrostatic interactions are the main reason of VESs viscosity impairment [69].

Objectives

The objective of the present research is to characterize the potential interactions/ reactions between VES-based solutions and common additives and contaminations in the well system, including corrosion inhibitors and cationic metals. The possible interaction or reaction of corrosion inhibitor packages, mainly the solvents because of their high concentrations, with different types of VES solutions will be characterized at a molecular level. Results will then be coupled with the viscosity and corrosion data to demonstrate how these reactions/interactions may affect the macroscopic properties of VES-based acid systems, including rheological behaviors and corrosion-inhibition performance. A characteristic study will also be done to determine the interaction of iron with the tested VES and to evaluate the conditions under which iron affects VES-based acid systems.

These results can be used to predict the incompatibility between different additives and contaminations in VES-based stimulation fluids and the possible occurrence of formation damage within the reservoir. Furthermore, these data can be employed to design VES-based stimulation fluids with improved performance and lower possibility of post damage in the formations.

CHAPTER II

MATERIALS AND METHODS

Materials

C22-tailed amidosulfobetaine surfactant, 3-(N-erucamidopropyl-N,N-dimethyl ammonium) propane sulfonate (EDAS) was synthesized according to the literature method [58]. An industrial nonionic (C_{22} long-chain N-oxide) VES and functionalized multiwalled CNT (Figure 1) were used as received. 3-sulfopropyldimethyl-3-methacryl-amidopropylammonium (SMA) was obtained from Arctom Chemicals (Figure 2). HCl (Macron, 36.5-38% with Fe < 0.1 ppm), deuterated hydrochloric acid (DCl, Cambridge Isotope Laboratories, 99.5%), deuterium oxide (D_2O, Cambridge Isotope Laboratories, 99.9%), dimethyl sulfoxide (DMSO, Cambridge Isotope Laboratories, 99.9%), $FeCl_3$ (Riedel-de Haën), and dihydrate calcium chloride (ACS grade, BDH) were used as received.

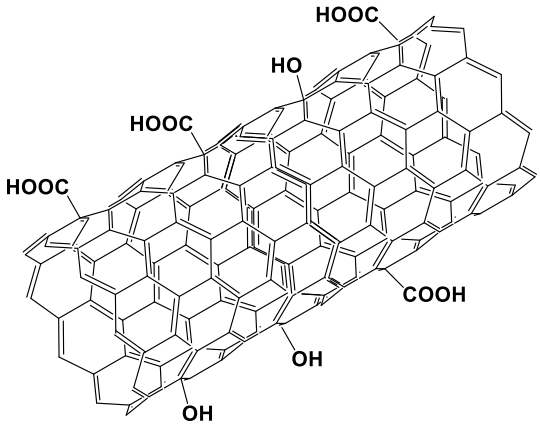

Figure 1. Functionalized Multiwalled Carbon Nanotubes (CNT)

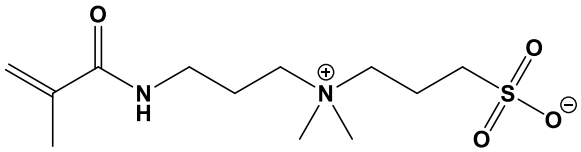

Figure 2. Chemical structures of 3-sulfopropyldimethyl-3-methacryl-amidopropylammonium (SMA)

Methods

Sample Preparation

VES and $FeCl_3$ Solutions

A solution of the desired amounts of $FeCl_3$ (60 mM) in HCl was first prepared, and then the desired concentration of substrate (EDAS or SMA) was added and gently agitated until a homogeneous solution was obtained. All samples were left at room temperature for 24 hours before measurements. The pH of the solutions was maintained at zero during the experiments.

VES and CNT Solutions

20 wt% dihydrate calcium chloride brine in deionized water was prepared, and then 0.02 to 0.2 wt% CNT was added and sonicated until complete dispersion and acquiring a homogenous solution. Afterward, 6 wt% VES was added to the solution and mixed for 15 minutes to have a homogenous mixture. Solutions were centrifuged at 5000 rpm for 15 minutes to extract entrapped air bubbles before any measurements. For the prevention of hydrogen-deuterium exchange, DMSO-d6 was used for some tests as the NMR solvent.

VES and Corrosion Inhibitors Solutions

To conduct visual tests, a solution of 15 wt% HCl acid, 4 wt% VES, and 1 wt% corrosion inhibitor was prepared, and the images were taken immediately after preparation at ambient conditions to avoid hydrolysis of VES. To conduct viscosity measurements, 20 wt% calcium chloride dihydrate brine in deionized water was prepared to improve the viscosity profile of the tested surfactants by initiating wormlike micellar structures in the solution. Then 4 wt% VES was added and mixed until complete solubilization and acquiring transparent homogenous solutions. After that, 1 wt% corrosion inhibitor was added to the solutions and mixed to have homogenous mixtures. Solutions were centrifuged at 5,000 rev/min for 15 minutes to extract entrapped air bubbles before any measurements. The pH of the tested solutions was neutral at equilibrium. The reason for conducting all viscosity tests in the present study with deionized water, without the addition of any acids, is to avoid interference of VES hydrolysis with the effects of mixing with corrosion inhibitors [70].

Rheological Measurements

Rheological measurements were carried out on an M5600 rotational rheometer (Grace Instrument) using a Hastelloy (HCl corrosion resistant) concentric cylinder geometry with a measuring bob radius of 1.5987 cm and a measuring cup radius of 1.7192 cm. The shear rate was varied in the range of 0.07 to 100 s^{-1} in the steady flow viscosity measurements, and the angular frequency was varied in the range of 0.1 to 30 s^{-1} in the dynamic viscoelasticity measurements. All the measurements were performed at 25.1 $\pm$ 0.1 °C and 2.75 MPa to minimize water evaporation.

Surface tension measurements were carried out using a Krüss K100 tensiometer by the automatic model of the du Noüy Ring technique. The cover was used to have minimum water evaporation. The measurements were taken until the equilibrium surface tension change became less than 0.03 mNm^{-1} every two minutes, and then the average of six measurements was reported.

Small angle X-ray scattering (SAXS)

Small-angle X-ray scattering (SAXS) experiments were performed using a Rigaku S-MAX-3000. Cu K_α X-rays (0.154 nm) were generated from an RA-Micro7 HFM tabletop rotating anode generator operating at 40 kV and 30 mA. The point-collimated beam was obtained using Rigaku Confocal Max-Flux^{TM} (CMF) optics. DCl and D_2O were used to prepare samples to reduce incoherent scattering. Solutions were deposited and sealed in capillary tubes, which were then mounted on an aluminum sample holder and illuminated at normal incidence in a vacuum at room temperature.

SAXS data were recorded using a two-dimensional single-photon counting detector with a pixel size of 100 μm at a sample-to-detector distance of 1.5 m. The detection q-range with this set-up is 0.08 to 2 nm^{-1}. Each sample was measured for 60 minutes, and then the sample was removed, after which background data were recorded for 60 minutes. 2D spectra were converted into 1D plots with azimuthal angle integration in SAXSGUI software, producing the scattering intensity profile I(q). The 1D background profile was subtracted from 1D solution sample profile. The magnitude of the scattering vector, q, is given by:

$$q = \frac{4\pi \sin(\theta)}{\lambda} \quad (4)$$

where θ and λ are half of the scattering angle and wavelength, respectively.

Infrared (IR) spectroscopy

IR spectra of the solutions were taken on a Thermo Nicolet 380 FTIR spectrometer in the absorption mode. All analyses were carried out at room temperature and resolution of 4 cm^{-1}, 64 scans, and over the wavenumber range of 600- 4000 cm^{-1}.

Nuclear Magnetic Resonance (NMR) Spectroscopy

NMR spectroscopy was carried out using a Bruker Advance 400 FT NMR (399.59 MHz for 1 H), and 1 H NMR chemical shifts δ are given in ppm and referenced against the solvent signals (TMS at 0 ppm). For the prevention of hydrogen-deuterium exchange for all tests, DMSO-d6 was used as the NMR solvent.

Ultraviolet-visible (UV-Vis) Spectroscopy

UV-visible measurements were carried out using a Genesys 10UV 145 spectrophotometer with a quartz cuvette of 1 cm path length in the wavelength range of 200-800 nm.

Single Crystal X-ray

SMA concentrated solution (700 mM) with 60 mM $FeCl_3$ in HCl was mixed and slowly evaporated to produce yellow crystals. A well-qualified crystal was chosen under

a polarized microscope and mounted to the X-ray instrument. Single crystal X-ray diffraction data were collected on a Bruker Quest diffractometer using Mo Kα radiation (λ = 0.71073 Å), cooled to 110 K using a cold nitrogen stream (Oxford). Integrated intensity information for each reflection was obtained by reduction of the data frames with the program APEX2. The integration method employed a three-dimensional profiling algorithm, and all data were corrected for L_p and decay. Finally, the data were merged and scaled to produce a suitable data set. The absorption correction program SADABS27 was employed to correct the data for absorption effects. The absence of additional symmetry and voids were confirmed using PLATON (ADDSYM). The structure was solved using SHELXS-2013 and refined using SHELXL-2013 with the Olex2 software package. All non-hydrogen atoms were refined with anisotropic thermal parameters. This Structure is deposited in the Cambridge Crystallographic Data Centre (CCDC) with number 1953033.

Corrosion Test

To conduct a corrosion test, 700 cm^3 of HCl (15%) containing 1% of a selected corrosion inhibitor, and 4% VES (if any) was placed in a Series 4523 1 L Hastelloy B benchtop reactor. Two coupons (L-80 and Cr-13) were weighted, dimensioned, and hung in a Hastelloy reactor. The sealed reactor was purged with nitrogen three times at 400 psi and then pressurized for 400 psi. The reactor was heated to 200±5°F for one hour (from starting time). After that, the reactor cooled with water and depressurized slowly. Coupons were washed with DI water and acetone. Dried coupons were weighted, and corrosion rates were calculated based on the following equation:

$$Corrosion\ rate\ \left(\frac{lb}{ft^2.h}\right) = \frac{Initial\ Mass\ -\ Final\ Mass}{Surface\ Area\ \times\ time} \quad (5)$$

CHAPTER III

INTERACTION OF IRON (III) WITH VES-BASED STIMULATION FLUIDS*

Physical Behavior of VES-Based Solutions in the Presence of Iron (III)

EDAS was soluble in HCl at the concentration of 30 mM, and the mixture was transparent and homogeneous. Because of the Z isomer for double bond and resulting kink in its erucyl tail, one might expect low T_k and high solubility of EDAS in water. However, EDAS low solubility (high Krafft temperature (T_k)) in water has been reported in the previous study and corresponded to its long hydrophobic tail and the inner nature of its sulfobetaine headgroup. It was also reported that the addition of NaCl led to the enhancement of EDAS solubility in water [71]. The solubility issue was not observed in HCl because of the charge separation and resulting ionic hydration that led to decreasing T_k.

No significant alteration of solution viscosity was observed after the addition of EDAS to the acid. However, upon continuous addition of Fe^{3+}, up to 60 mM, to the solution of 30 mM EDAS in HCl, a remarkable increase in the apparent viscosity of the solutions was observed. Figure 3 shows the macroscopic appearance of EDAS/HCl solutions before and after adding 60 mM Fe^{3+}. The reported data signify the transitions from a water-like solution (Figure 3, left image) with low viscosity to a homogenous gel-

* Reprinted with permission from "Micellar growth and network formation in acidic solutions of a sulfobetaine zwitterionic surfactant triggered by an inorganic salt" by Afra, S. et al. 2020. Soft Matter, 16, 4494-4501, Copyright 2020 by Royal Society of Chemistry.

like solution (Figure 3, right image). The latter solution was able to trap air bubbles for a long period of time that indicates viscoelasticity, which was also reported previously [37]. The gel-like nature of EDAS/HCl/Fe^{3+} solution was confirmed by conducting an inverted bottle test, and the solution was able to bear its weight on a short time scale. Results of further rheological analyses on these mixtures are presented and discussed later.

Figure 3. Macroscopic appearance of EDAS (30 mM)/HCl (5 M) solutions as a function of Fe^{3+} concentrations. (Left) no Fe^{3+}, and (Right) 60 mM Fe^{3+}.

The transition of the visual appearance of the EDAS/HCl/Fe^{3+} solutions can be attributed to the morphology of the micelles in these mixtures. Adding Fe^{3+} to the EDAS/HCl solution led to the entanglement of wormlike micelles that consequently induced viscoelasticity in the solution. The mechanism of morphology transition can be identified by investigating the precursors in the solutions, including EDAS and Fe^{3+} in

HCl. Such a transition can be attributed to the intensive interaction of Fe^{3+} species and surfactant, which will be described later in this chapter.

Morphological and micellar structural alteration in the solutions of multivalent ions such as Mg^{2+}, Zn^{2+}, $Al^{3+,}$ and surfactants has been reported previously. [72] Yet, the tested surfactant in the mentioned study was an anionic surfactant. In zwitterionic systems, including EDAS, it was assumed that because of the neutral charge of the headgroups, they are insensitive to the salts. [20,71] However, the present study shows that the addition of Fe^{3+} can prompt morphological transformation in the EDAS/HCl system.

Rheology of Fe (III) and VES Solutions

Figure 4 depicts the behavior of steady shear viscosity as a function of shear rate for the solutions of EDAS (30 mM)/HCl (5 M) before and after the addition of 60 mM Fe^{3+}. A low viscosity plateau was observed at low shear rates, and the viscosity rose with decreasing shear rate. Both solutions illustrated non-Newtonian shear-thinning behavior over the tested shear rates. Such a shear-thinning behavior can be attributed to either alignment of long micellar structures with the shear flow direction [37] or gradual breakage of long wormlike micelles with the increase of external forces. Since Newtonian behavior was not detected in the tested range of shear rates, it can be confirmed that, in both solutions, wormlike micelles were already formed. These results also indicate that the addition of Fe^{3+} (60 mM) to the EDAS/HCl solution increased viscosity approximately one order of magnitude. Such an increase in viscosity can be attributed to the formation of longer wormlike micelles and entanglement of these micelles into the transient network that led to the enhancement of viscoelasticity in the solution.

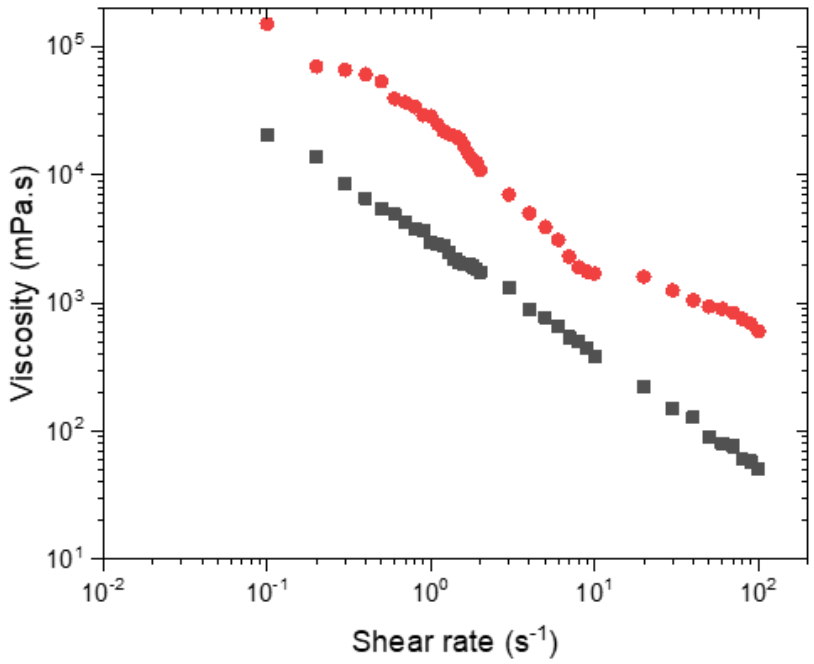

Figure 4. Steady shear viscosity as a function of shear rate for solutions of EDAS (30mM)/HCl (5 M) and EDAS (30mM)/HCl (5M)/Fe^{3+} (60mM)

Elastic behavior of EDAS and Fe^{3+} solutions in HCl was evaluated by dynamic rheological experiments using oscillatory-shear measurements. Figure 5 displays elastic modulus (G′) and viscous modulus (G″) as a function of angular frequency (ω) for solutions of EDAS (30mM)/HCl (5 M) before and after the addition of 60 mM Fe^{3+}. None of the solutions exhibited a viscous response since both moduli were independent of frequency, and G′ was greater than G″ over the tested frequency range. Figure 5 also shows that G′ and G″ never crossed over in the low-frequency ranges, which indicates a very long (infinite) relaxation time τ_R ($\sim 1/\omega_c$) for these solutions. Further, addition of Fe^{3+} to the EDAS/HCl solution led to an increase of plateau modulus G_0 by approximately one order of magnitude.

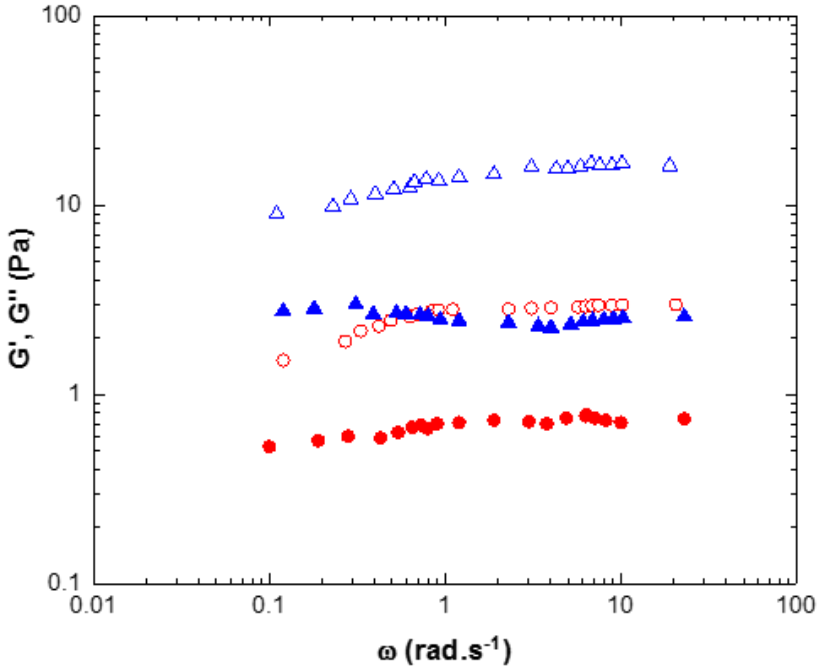

Figure 5. Dynamic Rheology of (Red) EDAS (30mM)/HCl (5 M) and (Blue) EDAS (30mM)/HCl (5M)/Fe^{3+} (60mM). Elastic modulus G' (unfilled symbols) and viscous modulus G″ (filled symbols) are plotted as a function of angular frequency

Generally, entangled wormlike micelles exhibit Maxwellian behavior at low shear frequency. However, none of the tested solutions in this study follow Maxwellian equations. These gel-like solutions stipulate infinite relaxation time and viscosity, and they are more similar to cross-linked polymer gel than to entangled, wormlike micelles.

Effects of Fe (III) on the Packing Parameter of VES-Acid System

The present work also investigated the effects of Fe^{3+} on the value of the EDAS packing parameter. To do so, the Gibbs adsorption equation was used to determine the surface excess concentration at the critical micelle concentration (Γ_{CMC}):

$$\Gamma_{CMC} = \frac{10^{20}}{N_A A_{min}} = -\frac{1}{2.303nRT}\left(\frac{\partial\gamma}{\partial(\log C)}\right)_T \quad (6)$$

Therefore, one may calculate A_{min} with the following equation:

$$A_{min} = -\frac{2.303nRT \times 10^{20}}{N_A\left(\frac{\partial\gamma}{\partial(\log C)}\right)_T} \quad (7)$$

Surface tension measurements of EDAS/HCl/Fe^{3+} system revealed specific features. First of all, as expected, EDAS/HCl solution exhibited very low CMC values (2.87×10^{-3} mN/m) because of the weak repulsion forces between headgroups (because of its zwitterionic nature) that led to easier formation and assembly of micelles. [71] Moreover, CMC value dropped to 0.98×10^{-3} mN/m after the addition of 60 mM Fe^{3+}. This decrease can be attributed to the introduction of Fe^{3+} to the system, which makes micelle formation more favorable. Furthermore, the surface tension measurement results show that adding 60 mM Fe^{3+} to the EDAS/HCl solution decreased the value of A_{min}. Based on the packing parameter formula, lowering the area per surfactant molecule increases the value of *P* that may be an indication of longer wormlike micelles formation.

Effects of Fe (III) on the SAXS Profile of VES System

For complementary structural analysis, SAXS measurements were carried out. Figure 6 shows the scattering profiles, scattering intensity (*I*) as a function of the scattering vector (*q*), of the solutions of EDAS (30 mM)/DCl (5 M), and EDAS (30 mM)/DCl (5 M)/Fe^{3+} (60 mM). At the low *q* region, scattering intensity follows $q^{-1.4}$ and q^{-1} dependence

for EADS/DCl and EDAS/DCl/Fe^{3+}, respectively. This type of scattering behavior is characteristic of a solution containing cylindrical wormlike micelles. [18,73–75] Besides, the position of the distinctive peak q^* at the high q region corresponds to the width of the wormlike micelles. Qualitatively, the slight increase of q^* position for EDAS/DCl/ Fe^{3+} suggests that the addition of Fe^{3+} can lead to the formation of thinner wormlike micelles.

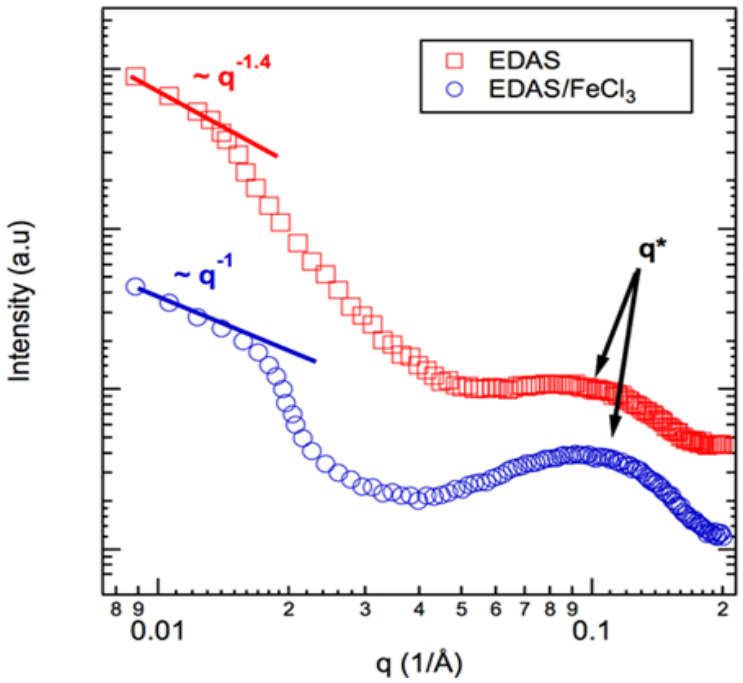

Figure 6. SAXS profiles of solutions of (red) EDAS (30 mM)/DCl (5 M) and (blue) EDAS (30 mM)/DCl (5 M)/Fe^{3+} (60 mM).

Mechanism of Wormlike Micelles Formation in the Presence of Fe (III)

IR Spectroscopy Results

Figure 7 shows the IR patterns of EDAS (30 mM) in HCl (5 M). The peak at 1635 cm^{-1} is representative of the C=O stretching vibration of the amide group. The peaks at 1550 and 3334 cm^{-1} can be assigned to N-H bending and stretching vibrations,

respectively. The peak at 1039 cm^{-1} can be attributed to the SO_3^- symmetric stretching modes. The EDAS solution contains water and ethanol with peaks that may overlap with N-H and SO_3^- signals. However, for the interaction between Fe^{3+} and EDAS/HCl solution, the C=O stretching vibration of the amide group can be monitored because no other peaks appeared in that region.

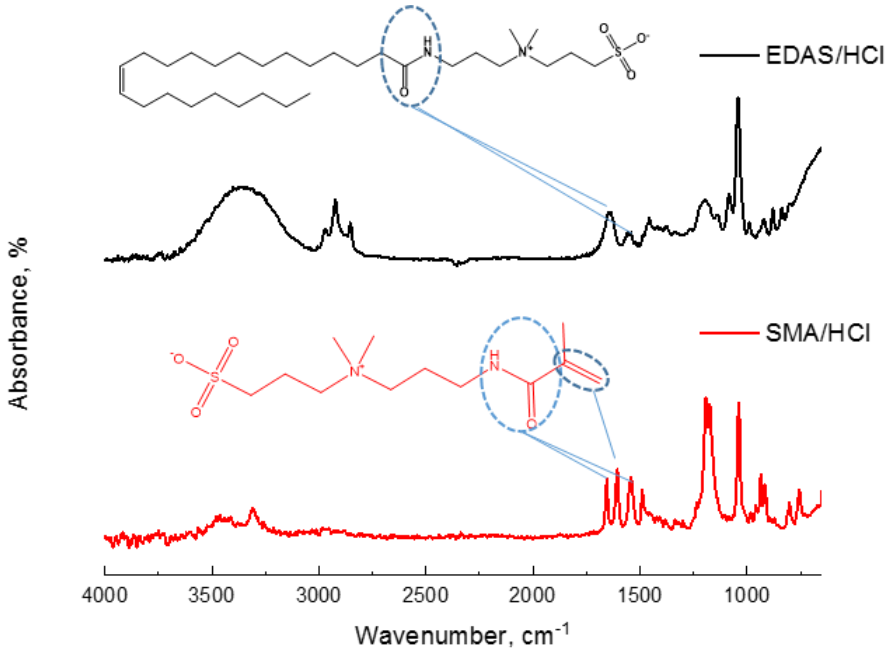

Figure 7. IR spectra of (top) EDAS (30 mM)/HCl (5 M) and (bottom) SMA (30 mM)/HCl (5 M)

After adding 60 mM Fe^{3+}, a notable shift in the IR spectrum could be recognized at 1635 cm^{-1} signal (C=O in amide). This peak shifted toward 1625 cm^{-1} gradually as the concentrations of Fe^{3+} increased. (Figure 8). Moreover, the second observed alteration of IR spectra was in the region of 3100-3700 $cm^{-1,}$ which is representative of N-H stretching. The third change that could be identified in the region of 1150-1250 cm^{-1} is that after the

addition of Fe^{3+}, this sharp peak became broader, indicating skeletal C-H waging with C-N stretching. These results confirm the interaction between Fe^{3+} and EDAS at pH=0 and also stipulate that the interaction is mainly through the EDAS amide group.

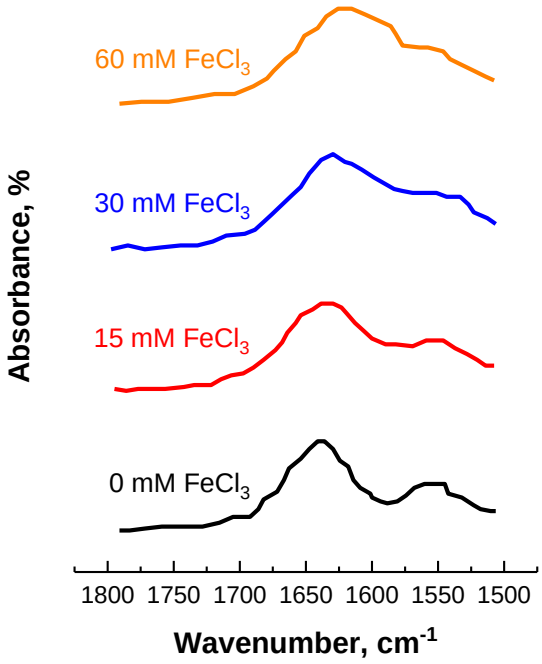

Figure 8. The C=O stretching vibration in IR spectrums of EDAS (30 mM)/HCl (5 M) solutions in the presence of (Black) no Fe^{3+} (red) 15 mM Fe^{3+} (blue) 30 mM Fe^{3+} and (orange) 60 mM Fe^{3+}

For a better understanding of the interaction between EDAS and Fe^{3+} and eliminating the interference of the EDAS tail group and solvent signals, SMA (the compound with the same headgroup as EDAS and without its long alkyl tail) was chosen as EDAS model compound. Similar spectroscopy tests were conducted on the solutions of SMA (30 mM)/ HCl (5 M)/ Fe^{3+} (60 mM) to validate the results of IR experiments on EDAS. Figure 7 shows the IR spectrum of SMA in HCl with the peak assignments. The peak at 1654 cm^{-1} is representative of the C=O stretching vibration of the amide group.

The peaks at 1548 and 3316 cm^{-1} indicate the N-H bending and stretching vibrations. These peaks can be detected in the EDAS IR spectrum as well. The peaks at 1606 and 1490 cm^{-1} are indicative of C=C symmetric and asymmetric stretching vibrations. These peaks were not observed in the EDAS IR spectrum because they were covered by the C=O stretching vibration.

Moreover, their nature is different, SMA has terminal alkene with a sharp signal at a lower frequency (~ 1600 cm^{-1}), and EDAS has internal alkene with a medium IR signal at higher frequencies (approximately 1650 cm^{-1}). The peak at 1041 cm^{-1} represents the distinctive sulfonate stretching vibration. After the addition of Fe^{3+} (60mM) to the SMA/HCl solution, the C=O stretching peak was shifted 10 cm^{-1} to the right, which indicates a change in the amide functional group of SMA. A slight shift was also noted after the introduction of Fe^{3+} to the solution of SMA/HCl in N-H bending vibration of the amide group. Another shift can be detected in the region of 1150-1250 cm^{-1}, which indicates skeletal C-H waging and C-N stretching vibrations.

Single Crystal X-ray

To better understand the interaction between Fe^{3+} and EDAS, extensive efforts have been made to make a single crystal suitable for X-ray analysis. However, because of the flexibility of the carbon chain that prevents the growth of a well-organized single crystal, there was no success in growing suitable single crystal for analysis. Therefore, SMA has been selected as a model compound for EDAS that has no flexible carbon chain. SMA concentrated solution (650 mM) with 240 mM Fe^{3+} in HCl was slowly evaporated to produce yellow crystals that were appropriate for X-ray measurement. A well-formed

crystal was chosen under a polarized microscope and mounted to an X-ray instrument with Mo source. After collecting the data and solving the structure, *trans*-$[FeCl_2(H_2O)_4]Cl$ was detected for the tested crystal (Figure 9). The structure shows that chloride counterion has a hydrogen bonded with one of the coordinated water molecules, and no binding between SMA and Fe^{3+} center in the solid state was detected. Although the hydrogen bond through the chloride ion (Cl^-) is very weak and rare, a partially strong hydrogen bond can be observed in the reported structure based on the 2.327 Å bond length of Cl···H.

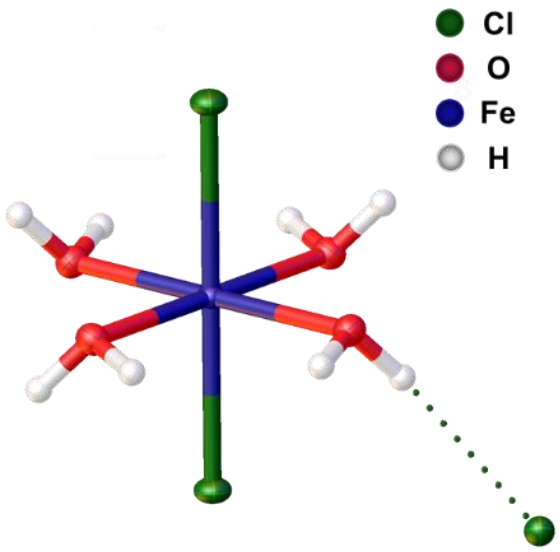

Figure 9. Ellipsoid of trans-$[FeCl_2(H_2O)_4]Cl$ single crystal structure that was measured at 110 K

The nature and geometry of aqueous $FeCl_3$ species at different chloride concentrations and pH values have been thoroughly investigated. [76–78] $[Fe(H_2O)_6]Cl_3$, $[Fe(H_2O)_5Cl]Cl_2$, and $[Fe(H_2O)_4Cl_2]Cl$ share an octahedral geometry. $[FeCl_3(H_2O)_n]$, n =

1 or 2, could be either tetrahedral or trigonal bipyramidal, and $[FeCl_4]^-$ is expected to be tetrahedral. At room temperature and without adding an external chloride source, extended X-ray absorption fine structure (EXAFS) data suggest that aqueous $FeCl_3$ may be a mixture of octahedral and tetrahedral or trigonal bipyramidal forms. [76]

In the absence of a chloride source, $FeCl_3$ exists as $[Fe(H_2O)_6]Cl_3$ with λ_{max} = 240 nm. Depending on the chloride concentration and pH, $[Fe(H_2O)_5Cl]Cl_2$, $[Fe(H_2O)_4Cl_2]Cl$, and ultimately $[FeCl_4]^-$ with higher absorbance constant may be formed. At a chloride concentration of 0.3 to 4 M, the major component is $[Fe(H_2O)_5Cl]Cl_2$, and in the concentration range of 4 to 9 M, the dominant species is $[Fe(H_2O)_4Cl_2]Cl$, and above 15 M and at elevated temperatures, such as 90°C, $[FeCl_4]^-$, is the major component. [76] Based on the HCl concentration (5 M) in the present study and the results of theoretical calculations and experimental studies, the major component is expected to be $[Fe(H_2O)_4Cl_2]Cl$. [76–78] The results of single crystal X-ray analysis confirm the existence of the proposed structure and provide more supplementary information about this component, such as exact geometry, e.g., *cis* or *trans*, non-coordinated chloride position, and interaction between ions.

UV-Vis Spectroscopy

To further confirm that the *trans*-$[FeCl_2(H_2O)_4]Cl$ is the dominant component in the solution state at the tested experimental conditions, the measured single crystal was redissolved in HCl, and its UV-visible absorbance was analyzed and compared to the absorbance of predicted structures in previous studies [76–78], and the absorbance of the solution of $FeCl_3$ (0.1 mM) in HCl (5 M) used to conduct the experimental study in the

present work. All three absorbance spectra demonstrated identical signals at 335 nm and below 250 nm that correspond to the presence of *trans*-$[FeCl_2(H_2O)_4]Cl$ as a dominant component in the tested solutions. Upon addition of EDAS to these solutions, the distinctive signals at 335 and 250 nm disappeared, and a new component with a signal at 278 nm was formed. This observation agrees with the IR results exhibiting the interaction between EDAS and Fe^{3+} in HCl.

Discussion

According to the results of IR, UV-Vis, and single crystal X-ray spectroscopy techniques, the entanglement of wormlike micelles after the addition of Fe^{3+}, which was confirmed by rheology results, can be attributed to the intensive interaction of Fe^{3+} and EDAS in acidic conditions. The results of IR spectroscopy indicate that the primary interaction between Fe^{3+} and EDAS is through the amide group (because of the shifts in amide IR signals). In general, amides barely participate in reactions as ligands for metals, and even as a ligand, they may weakly bind to the metal ions and act as leaving groups. [79] For instance, N,N-dimethylformamide (DMF) is known as an amide with the ability to participate in both coordination reaction with metal ions and weak interactions such as hydrogen bonding. Upon its coordination through oxygen, significant shifts in C=O stretching vibrations toward lower frequencies, around 20-30 cm^{-1}, were reported. [80] Moreover, in the case of coordination and the presence of an excess amount of DMF, two signals, coordinated and free amides, could be detected. On the contrary, when DMF was involved in weak interactions such as hydrogen bonding, C=O stretching vibrations were expected to undergo a gradual shift, around 5-17 cm^{-1}, toward lower frequencies. [81]

In the present study, because of the presence of gradual shifting in the amide C=O stretching vibration and the absence of two amide signals (coordinated and non-coordinated), one may conclude the existence of hydrogen bonding, not a coordination reaction. Additionally, single X-ray crystallography results asserted no direct bonding between amide oxygen and Fe^{3+} and confirmed the presence of *trans*-$[FeCl_2(H_2O)_4]Cl$ complex that is capable of forming hydrogen bonds with weak species such as an amide or chloride ions through more acidic and directional hydrogen in coordinated water. Such hydrogen bonding would result in the screening of the repulsion forces between surfactant headgroups and the formation of a system containing long wormlike micelles.

CHAPTER IV

EFFECTS OF CORROSION INHIBITORS ON VES-BASED STIMULATION FLUIDS*

Visual Tests

All the visual tests in this study were conducted at ambient conditions. In this entire chapter, the tested zwitterionic surfactant will be referred to as VES 1, and the nonionic surfactant will be referred to as VES 2. Figure 10 shows the mixture of VES solutions and corrosion inhibitors at a pH of zero. Solutions of VES 1 with corrosion inhibitors A and B were clear and homogenous. The solutions exhibited viscoelasticity and met the defined criteria for gel-like materials stating that if the sample is placed into a vial and overturned, it does not flow down over a time scale of at least minutes, which is a reflection that the material has yield stress [82]. However, the solution of VES 1 and corrosion inhibitor C was not clear, and phase separation occurred in the solution. Solutions of VES 2 also followed the same trend as solutions of VES 1; in the presence of corrosion inhibitors A and B, the solutions were clear and viscoelastic; however, upon addition of corrosion inhibitor C, two phases were formed without any viscosity. Results of the further rheological analysis of these mixtures are presented and discussed later in this chapter.

---

* Reprinted with permission from "NMR Investigation of Viscoelastic Surfactant Compatibility with Corrosion Inhibitors" by Afra, S. et al. 2020. SPE Journal, Preprint, Copyright 2020 by Society of Petroleum Engineers.

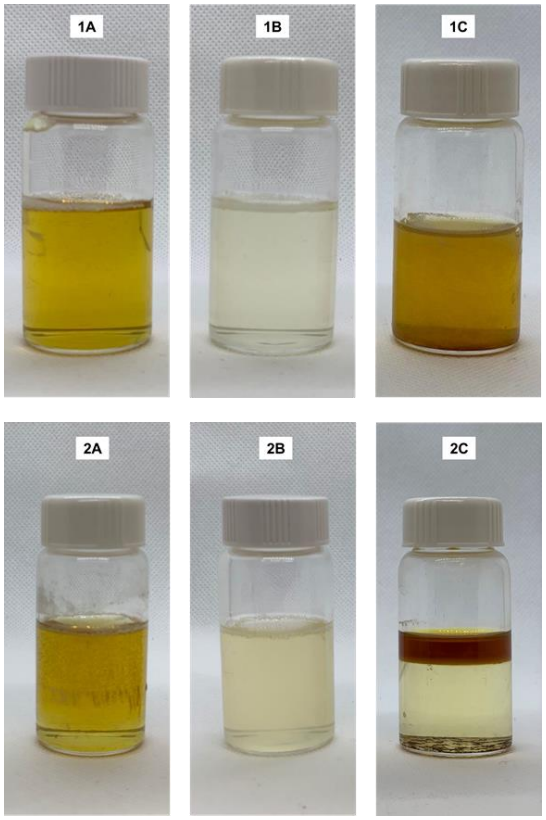

Figure 10. Visual appearance of solutions of (up) VES 1 and (bottom) VES 2 in the presence of tested corrosion inhibitors at ambient conditions.

Impact of Corrosion inhibitors on the Rheology of VES Systems

Figure 11 shows the results of rheological measurements on the solutions contained VES 1. The apparent viscosity of VES 1 without any additives demonstrated the typical response of VES-based systems. As the temperature increased, the sample started to build up viscosity until a certain temperature (210 °F), and then viscosity started to drop. Such a behavior has been attributed to the formation of wormlike micelles and a transient network of entangled wormlike micelles. [34] In this specific VES sample, another peak was observed in the plot of viscosity versus temperature. The existence of the second peak

may be because of the formation of branched wormlike micelles in this temperature range that led to an increase in the viscosity. [83]

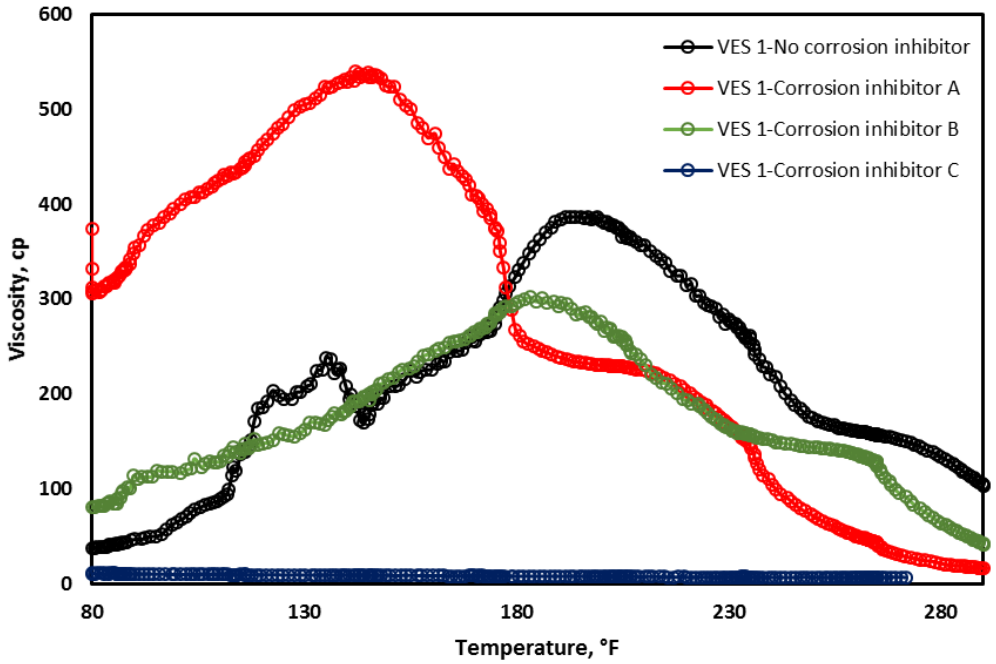

Figure 11. Viscosity of VES 1 (4 wt%) with three tested corrosion inhibitors (1 wt%).

After adding corrosion inhibitors to VES 1, various responses were observed (Figure 11). For the sample contained corrosion inhibitor A, below 180°F, a synergistic effect was noticed, which means the solution viscosity was more than that of the solution without corrosion inhibitor. However, when temperature passed 180°F, the viscosity began to drop gradually. Both peaks in the viscosity diagram of VES-corrosion inhibitor mixture were observed, but at the lower temperature compared to the sample without corrosion inhibitor. After the addition of corrosion inhibitor B to VES 1, the viscosity became lower in the entire temperature range tested; however, the overall behavior (two viscosity peaks over the tested temperature range) remained the same. For the corrosion inhibitor C, the VES

response was completely different; no viscosity was built up over the whole temperature range. Further analysis of these systems was done using NMR and will be explained later in this chapter.

Figure 12 illustrates the results of viscosity measurements for the systems that contained VES 2 and tested corrosion inhibitors. The main difference in the rheological behaviors of VES 1 and VES 2 was that the later one showed a single peak in its viscosity profile, while VES 1 had a viscosity profile with two peaks. This dissimilarity may be attributed to the fact that VES 2 cannot form a micellar system consists of branched wormlike micelles, which may be related to its chemical structure. According to the literature, nonionic surfactants would be able to form branched wormlike in the presence of a counterion or a co-surfactant [83], which is not the case in the tested solutions in this study.

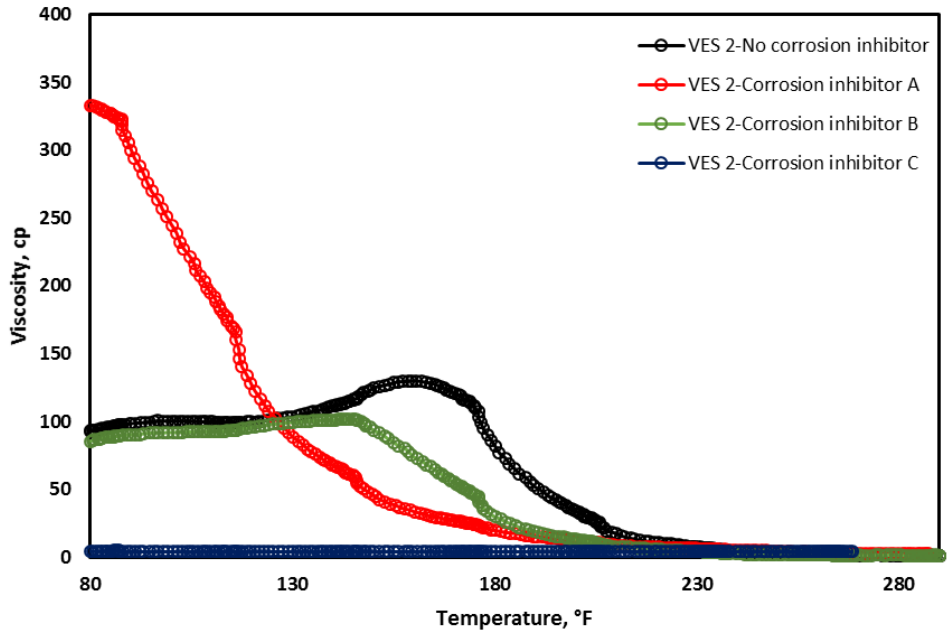

Figure 12. Viscosity of VES 2 (4 wt%) with three tested corrosion inhibitors (1 wt%).

The synergistic effect of corrosion inhibitor A on the viscosity of the VES solutions below 130°F was also observed in the VES 2 mixtures. However, the overall performance of VES 2 was impaired after adding corrosion inhibitor A. The response of VES 2 to corrosion inhibitor B in terms of viscosity performance can be compared with the response of VES 1. The viscosity was dropped slightly in the whole temperature range. The solution of VES 2 and corrosion inhibitor C showed low viscosity over the tested temperature range.

Characterization of the Interaction/Reaction of Corrosion Inhibitors with VES Solutions Using NMR Spectroscopy

Figure 13 shows the ^{1}H NMR spectrum of VES 1 at 78°F. These results indicate that VES 1 contains water, ethanol, and propylene glycol beside its active component, which is a zwitterionic surfactant. As shown in Figure 13, the singlet signal at 3.36 ppm represents a significant amount of water content. A set of signals at 1.05 (triplet), 3.44 (multiplet), and 4.37 ppm (triplet) with a ratio of 3:2:1 can be related to a CH_3 group, a CH_2 group, and an OH group of ethanol, respectively. A doublet at 0.99 ppm related to CH_3 group, two sets of doublet of doublet at 3.16 and 3.24 ppm can be assigned to an asymmetric CH_2 group, and a sextet at 3.55 ppm can be attributed to a CH group. A doublet at 4.42 ppm and a triplet at 4.48 ppm indicate the two hydroxyl (OH) groups of 1,2-propanediol (propylene glycol). These assignments are in good agreement with reported chemical shifts in the literature. [84] The remaining signals for this mixture are indicative of the zwitterionic surfactant.

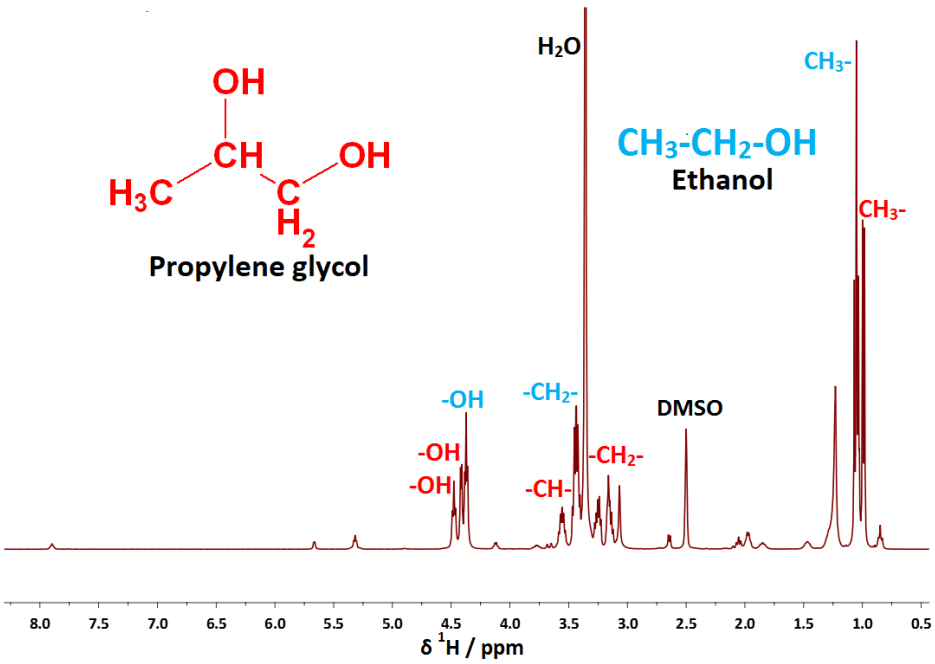

Figure 13. ^{1}H NMR of VES 1 in DMSO-d6 at 78°F

Figure 14 shows the ^{1}H NMR spectrum of VES 2 at 78°F. These results demonstrate that VES 2 contains propylene glycol as a solvent and a nonionic surfactant as an active agent. A singlet signal at 3.35 ppm represents water content. Small differences in the location of water peaks occur because the hydroxide signal position can be affected by the presence of solvents, other substrates, and temperature. A doublet at 0.99 ppm, two sets of doublet of doublet at 3.16 and 3.24 ppm, a sextet signal at 3.55 ppm, and a broad signal at 4.48 ppm with 3:1:1:1:2 ratio can be assigned to CH_3 group, asymmetric CH_2 group, CH group, and two hydroxyl (OH) groups of propylene glycol respectively. The remaining signals in this spectrum are related to the nonionic surfactant.

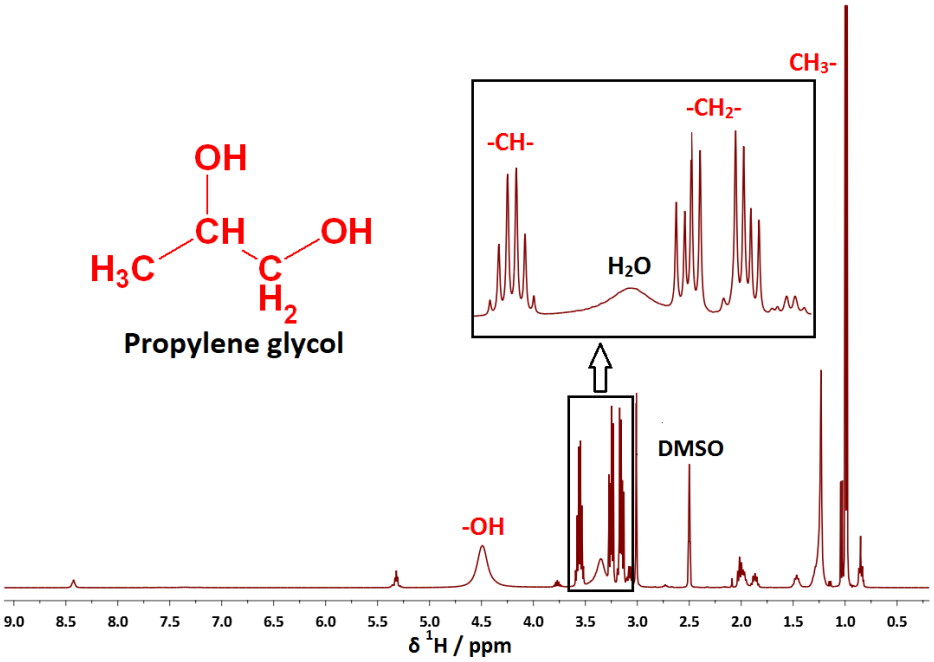

Figure 14. ^{1}H NMR of VES 2 in DMSO-d6 at 78°F

Figure 15 depicts the ^{1}H NMR spectrum of corrosion inhibitor A. This spectrum shows that corrosion inhibitor A contains water, which appeared as a broad signal at 3.38 ppm. Moreover, this corrosion inhibitor contains formic acid with two characteristic signals at 8.13 ppm, a sharp signal related to hydrogen that is attached to the carbonyl group, and a broad signal at 12.75 ppm, which referred to the OH group attached to carbonyl. In addition to water and formic acid, two sets of signals representative of a small amount of isopropanol, one doublet at 1.04 ppm of CH_3 groups, and a septet at 3.78 ppm of CH group, were observed. The remaining signals belong to the active components in the solution.

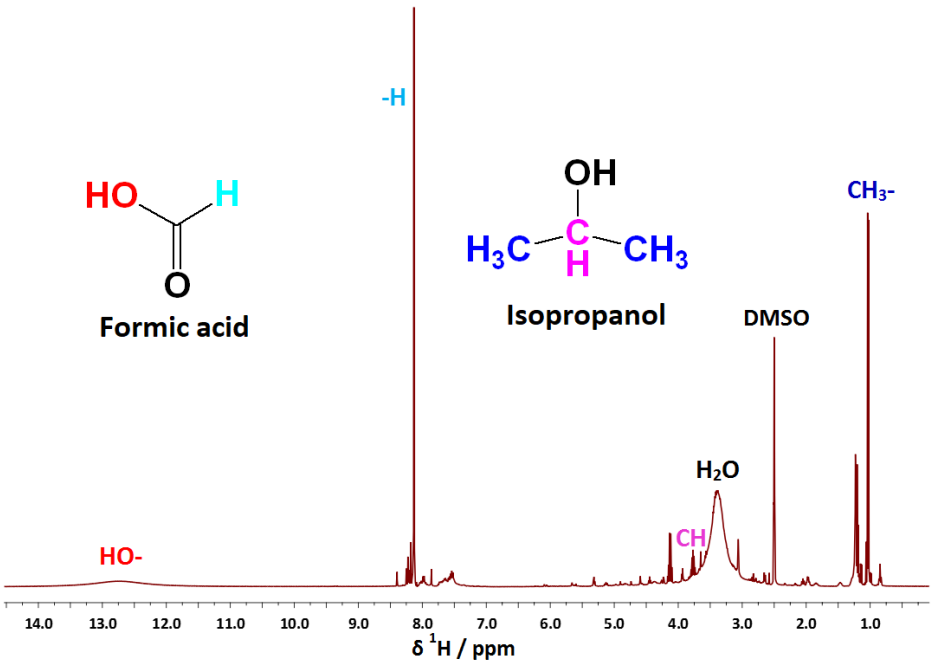

Figure 15. 1H NMR of corrosion inhibitor A in DMSO-d6 at 78°F

In the ^{1}H NMR spectrum of corrosion inhibitor B shown in Figure 16, a doublet at 1.04 ppm related to CH_3 groups and a septet at 3.78 ppm related to CH group confirm the presence of isopropanol in the solution. Beside isopropanol, methanol with two distinctive singlets at 3.17 for CH_3 group and 4.06 ppm for OH group can be detected. Minor components in this mixture that show signals in the aromatic region between 6.25 to 9.75 ppm can be related to active agents of corrosion inhibitor solution shown in the inset of Figure 16.

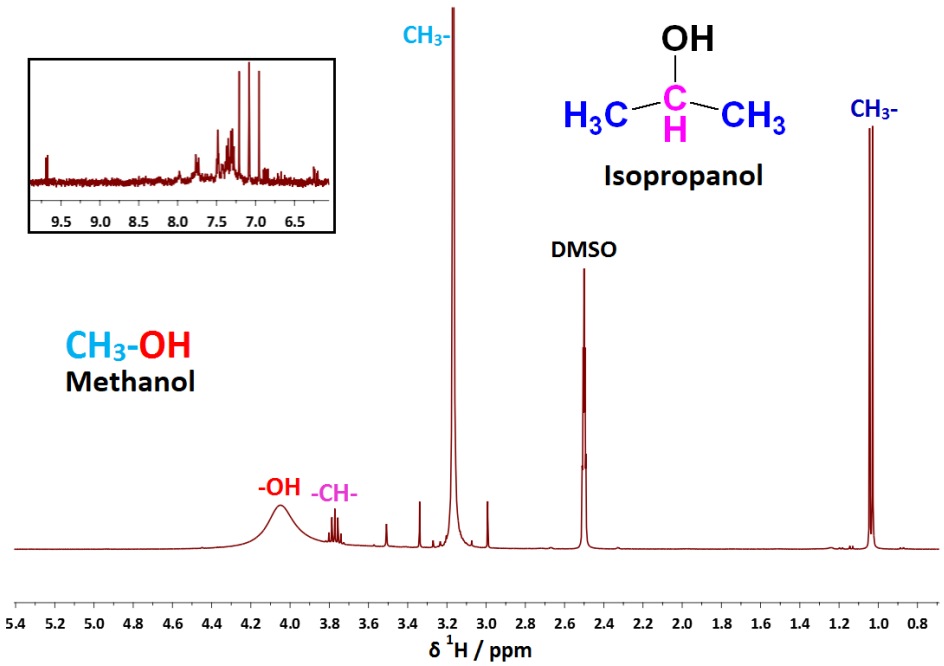

Figure 16. ^{1}H NMR of corrosion inhibitor B in DMSO-d6 at 78°F. The inset shows the peaks in the aromatic region for corrosion inhibitor B

Figure 17 shows the ^{1}H NMR spectrum of corrosion inhibitor C. A doublet at 1.04 ppm and a septet at 3.78 ppm can be assigned to CH_3 groups and CH group of isopropanol in the solution, respectively. A singlet at 1.91 ppm and a broad singlet at 11.97 ppm that can be related to CH_3 and OH groups are representative of acetic acid in the solution. A singlet at 2.59 ppm can be assigned to CH_3 group, and three sets of signals between 7.5-8 ppm (shown in the inset of Figure 17) can be attributed to ortho-, para-, and meta-protons belong to acetophenone. The remaining signals are related to corrosion inhibitor active agents.

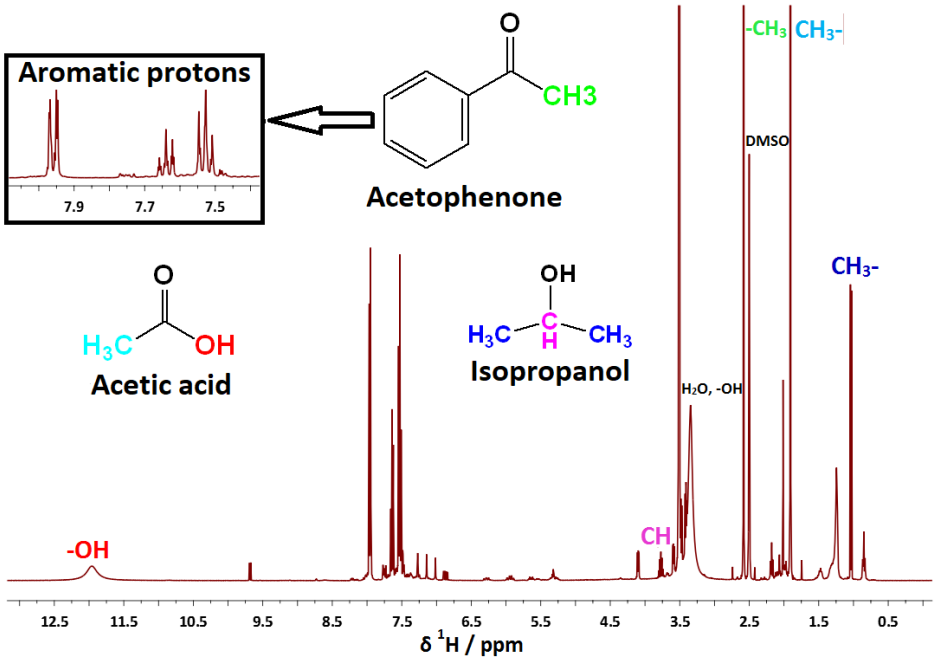

Figure 17. ^{1}H NMR of corrosion inhibitor C in DMSO-d6 at 78°F. The inset shows the peaks in the aromatic region for corrosion inhibitor C

NMR spectrum of the mixture of VES 1 and corrosion inhibitor A in the temperature range of 78-200°F did not show any significant reaction between system components (Figure 18). The synergistic effect of corrosion inhibitor in viscosity performance below 180°F can be related to the weak interaction of corrosion-inhibitor solvents and VES additives. The OH signals of formic acid and propylene glycol were shifted upfield, the OH signal of water shifted downfield, and the NH signal of VES shifted downfield slightly. All these signals could be detected as a single broad signal at 3.82 ppm at room temperature and 3.68 ppm after heating up for 24 hours.

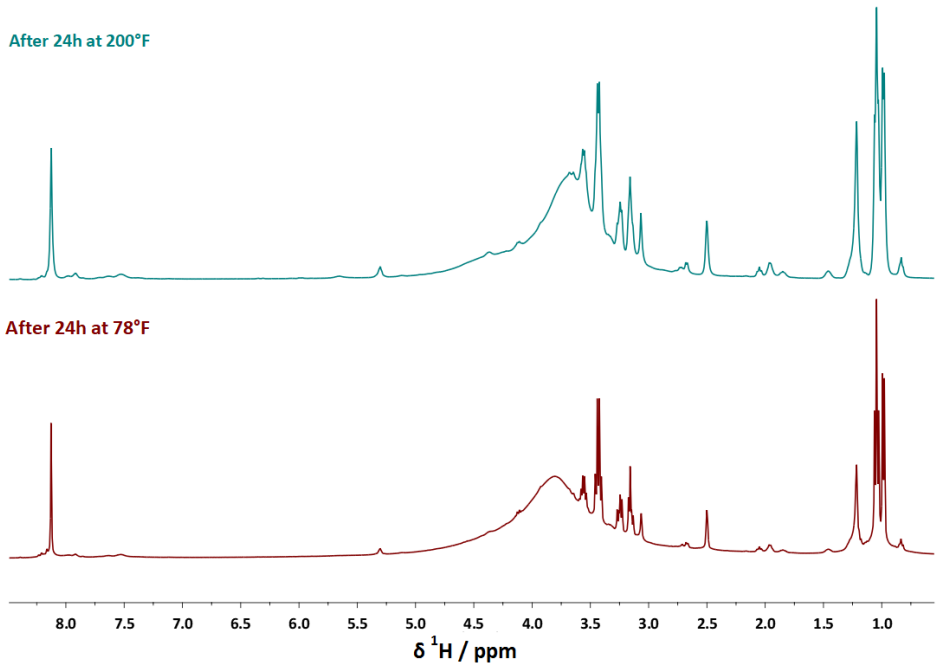

Figure 18. ^{1}H NMR spectra of the mixture of VES 1 and corrosion inhibitor A in DMSO-d6

VES 1, corrosion inhibitor B, and their mixtures are very stable in the temperature range of 78 to 200°F (Figure 19). Even after 24 hours at 78 and 200°F, no significant reaction between the components of the tested mixture was observed. The multiplet at 5.32 ppm and a broad singlet at 1.23 ppm did not change over time at the tested temperature range, which is indicative of the fact that VES 1 did not participate in any reaction. However, a water signal at 3.34 ppm and hydroxyl groups of different alcohols (signals between 4.35 to 4.50 ppm) shifted upfield, especially at elevated temperature (200°F). These shifts indicate that only OH groups of solvents such as water, methanol, ethanol, isopropanol, and propylene glycol had interactions with each other and appeared as a broad signal at 3.70 ppm.

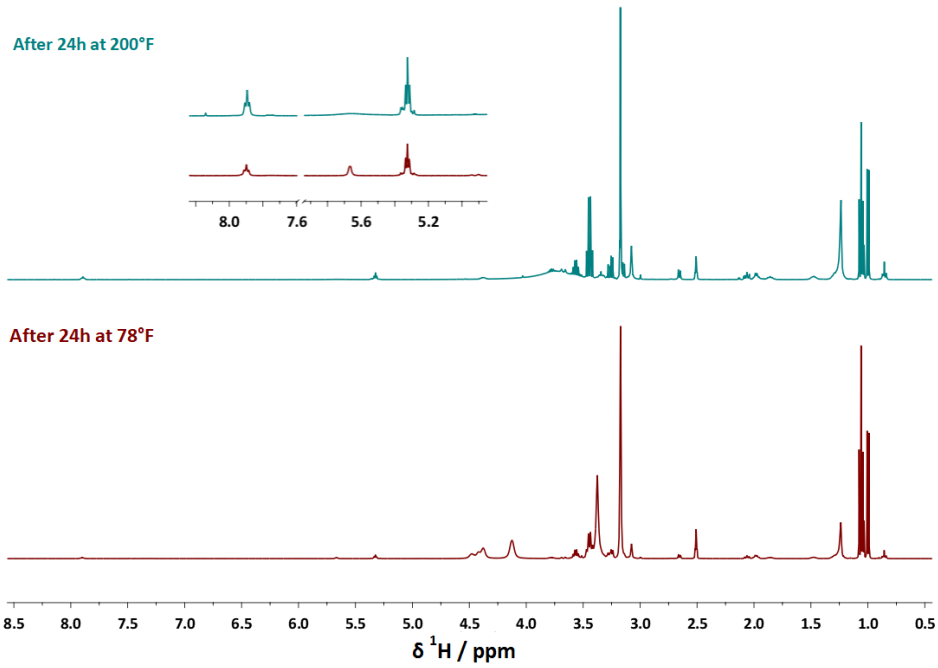

Figure 19. ^{1}H NMR spectra of the mixture of VES 1 and corrosion inhibitor B in DMSO-d6

As shown in Figure 20, notable changes can be observed in the NMR spectrum of the mixture of VES 1 and corrosion inhibitor C. The amide hydrogen in original VES 1, located at 7.90 ppm, disappeared upon mixing with corrosion inhibitor C that might be because of the partial decomposition of VES 1 at elevated temperatures (200°F). The decomposition of VES 1 can be further proved by the generation of new signals at higher temperatures. Additionally, the formation of some signals upon mixing of VES 1 and corrosion inhibitor C was observed that cannot be fully characterized because of the lack of enough data on corrosion inhibitor composition. The poor rheological performance of VES 1 in the presence of corrosion inhibitor C can be explained with these results as the decomposed VES cannot generate any viscosity in the solution.

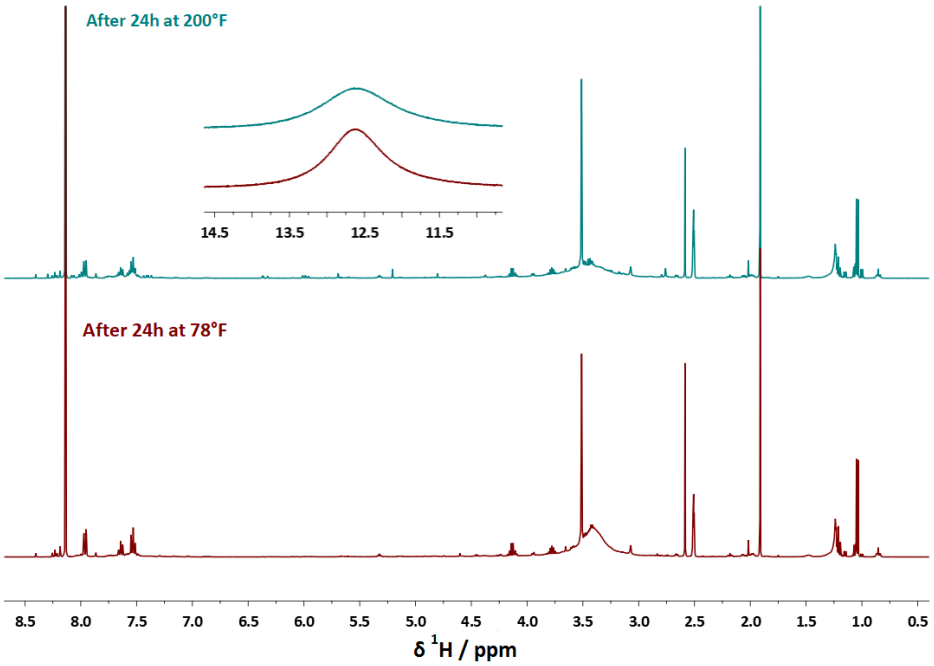

Figure 20. ^{1}H NMR spectra of the mixture of VES 1 and corrosion inhibitor C in DMSO-d6 at different temperatures

Figure 21 indicates the NMR spectrums of a mixture of VES 2 and corrosion inhibitor A at the tested temperature range. The hydroxyl group of alcohol and water in VES 2 (4.49 ppm) moved to 4.78 and 4.52 ppm at 78 and 200°F, respectively. VES 2 has a methylamine (NMe_2) group that initially appeared at 3.01 ppm and moved to 3.30 ppm at 78°F and to 2.46 ppm at 200°F. The hydrogen attached to the carbonyl group in formic acid, which originally was at 8.13 ppm in corrosion inhibitor A, moved to 8.23 ppm at 78°F and 8.25 ppm at 200°F. These shifts are indicative of the acid-base reaction of the amine functional group of VES 2 with formic acid in corrosion inhibitor A. The acid-base reaction between formic acid in corrosion inhibitor solution and amine functional group in VES may change the micellar structure and, subsequently, the viscosity. Since the acid-

base reaction is highly sensitive to temperature changes, such a reaction would impair the viscosity at high-temperature ranges.

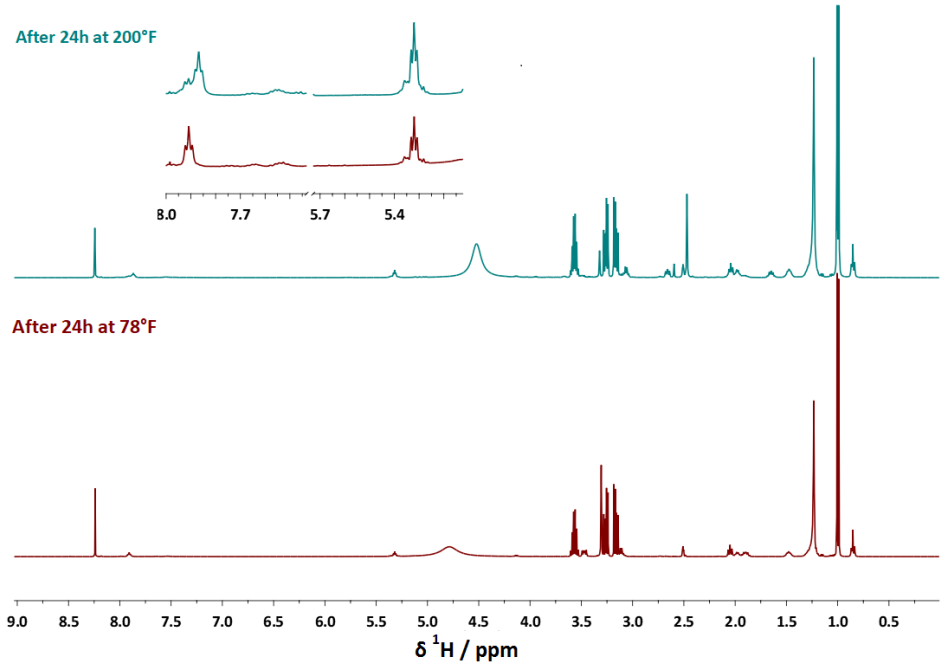

Figure 21. ^{1}H NMR spectra of the mixture of VES 2 and corrosion inhibitor A in DMSO-d6 at different temperatures

Figure 22 shows the ^{1}H NMR spectrum of VES 2 and corrosion inhibitor B mixture at 78 and 200°F. At 78°F, no significant reaction was detected, and only some weak interaction was observed. These weak interactions may be the reason for the slight viscosity drop observed in Figure 11. However, strong interactions, especially between the amide group in VES 2 and methanol in corrosion inhibitor B, can be detected at 200°F. These strong interactions led to viscosity impairment of VES 2 at higher temperatures. No sign of VES 2 decomposition can be detected from the NMR spectra.

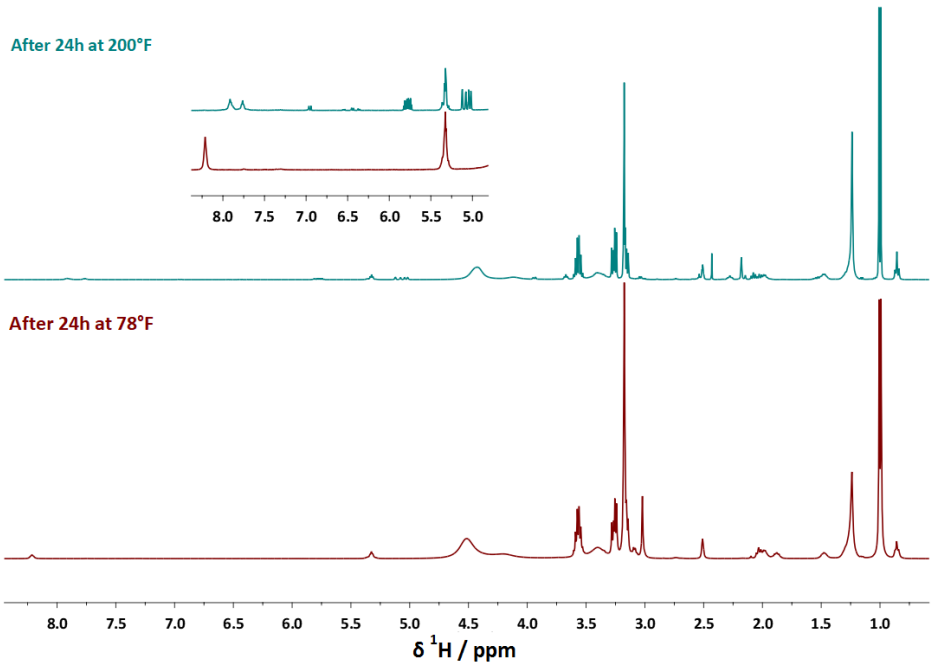

Figure 22. ^{1}H NMR spectra for the mixture of VES 2 and corrosion inhibitor B in DMSO-d6 at different temperatures

NMR spectrum of VES 2 and corrosion inhibitor C is shown in Figure 23. The decadence of amide group in VES 2 (signal at 8.43 ppm was disappeared) stipulate the partial decomposition of VES 2 in the presence of corrosion inhibitor C. Formation of a signal between 2 and 2.5 ppm may be because of the presence of additives in corrosion inhibitor C that cannot be detected using NMR. These observations can be further proven with rheological measurements so that no viscosity was observed in the mixture of VES 2 and corrosion inhibitor C. Such a rheological behavior was also observed in the mixture o VES 1 and corrosion inhibitor C.

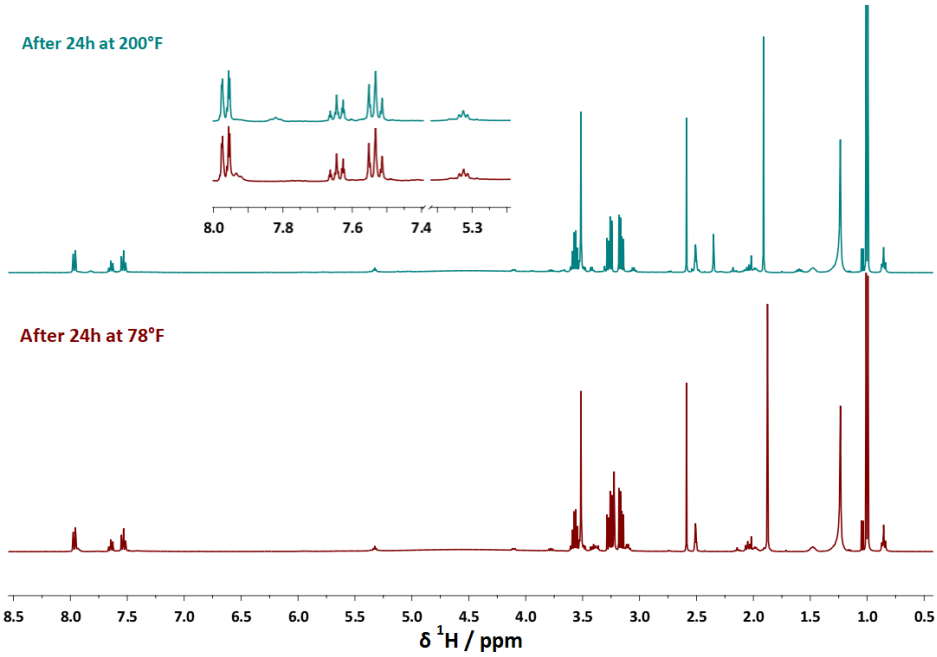

Figure 23. ^{1}H NMR spectra of the mixture of VES 2 and corrosion inhibitor C in DMSO-d6 at different temperatures

Effects of VES on Performances of Corrosion Inhibitors

Table 1 and Table 2 show the results of corrosion experiments for the tested corrosion inhibitors, VESs, and coupons. The results indicate that the corrosion rates of all three tested corrosion inhibitors are below the corrosion limits defined for Cr-13 and L-80 coupons. It can be seen from these tables that the addition of VES 1 to the solutions of corrosion inhibitors A and C slightly decreased the corrosion rates of both tested coupons. However, adding VES 1 to the acid impaired the performance of corrosion inhibitor B, and the corrosion rates increased slightly in both coupons. In the case of VES 2, the same behavior was observed; no significant change in the corrosion rate of corrosion inhibitors A and C was detected; however, the performance of corrosion inhibitor B was diminished notably in the L-80 coupon. The performance impairment of corrosion

inhibitor B in the presence of VES samples may be because of the strong interactions between VES and corrosion inhibitor samples that prevents the spread of corrosion inhibitors on the surface of the metal. However, it should be noted that even such an interaction would not reduce the performance of corrosion inhibitor B such that it does not pass the standard corrosion limit.

Table 1. Corrosion rates (lb./(ft^2.h)) for Cr-13 alloy

	No VES	**VES 1**	**VES 2**
Corrosion Inhibitor A	0.00055	0.00031	0.00054
Corrosion Inhibitor B	0.00021	0.00049	0.00076
Corrosion Inhibitor C	0.00021	0.00007	0.00015

Table 2. Corrosion rates (lb./(ft^2.h)) for L-80 alloy

	No VES	**VES 1**	**VES 2**
Corrosion Inhibitor A	0.00610	0.00291	0.00538
Corrosion Inhibitor B	0.00447	0.02799	0.01792
Corrosion Inhibitor C	0.00378	0.00243	0.00461

CHAPTER V

ENHANCEMENT OF THE PERFORMANCE OF VES-BASED FRACTURING FLUID WITH A NOVEL FUNCTIONALIZED CNT*

Viscosity Behavior of VES-CNT Systems

Two main concentrations of CNT, 0.02 and 0.2 wt%, were used to study the effects of CNT on the rheological behavior of VES solutions. In this entire chapter, the tested nonionic surfactant will be referred to as VES 1, and the zwitterionic surfactant will be referred to as VES 2. Figure 24 shows the viscosity diagram of VES 1 with different concentrations of CNT (0 to 0.2 wt%). The apparent viscosity of VES 1 without any additives demonstrated a typical response of VES-based systems. As temperature increases, the sample starts to build up viscosity until a specific temperature, and then after that, viscosity starts to drop. Such a behavior has been attributed to the formation of wormlike micelles and a transient network of entangled wormlike micelles. [34]

* Reprinted with permission from "A Novel Nanotube/VES-Based High Temperature High Pressure Fracturing Fluid" by Afra, S. et al. 2020. SPE International Conference and Exhibition on Formation Damage Control, Copyright 2020 by Society of Petroleum Engineers.

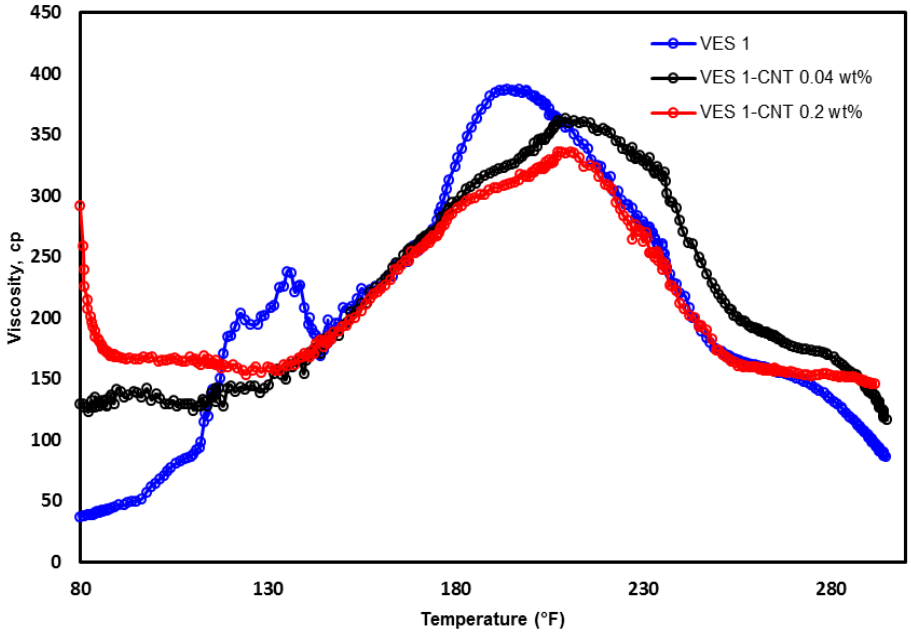

Figure 24. Viscosity profile of VES 1 in the presence of 0, 0.02 and 0.2 wt% CNT

These micelles would form following the weak interaction between the active surfactant and the additives such as propylene glycol in the VES solution. Temperature alteration is the primary trigger for these weak interactions that consequently affects the repulsion forces between surfactant headgroups and favors the generation of wormlike micelles in the solution. In this specific VES sample, another peak was observed in the plot of viscosity versus temperature. The existence of the second peak can be explained by the formation of branched wormlike micelles in this temperature range that led to an increase in the viscosity. [83]

After the addition of CNT to the VES 1 solution, various responses were observed in different temperature ranges. At low temperatures, below 120 °F, enhancement in viscosity were observed at tested CNT concentrations. In the temperature range of 140-185 °F, the same

performance was observed in all solutions; however, the maximum viscosity of the VES sample without any additives was determined to be slightly higher than the ones with CNT. One of the most important features of the VES viscosity profile in the presence of 0.2 wt% CNT was its stability and better performance at higher temperatures (higher than 185 °F). Such an observation can be confirmed with the results presented in Figure 25. The solution of VES 1- CNT (0.2 wt%) exhibited a stable viscosity profile at 300°F for 100 minutes.

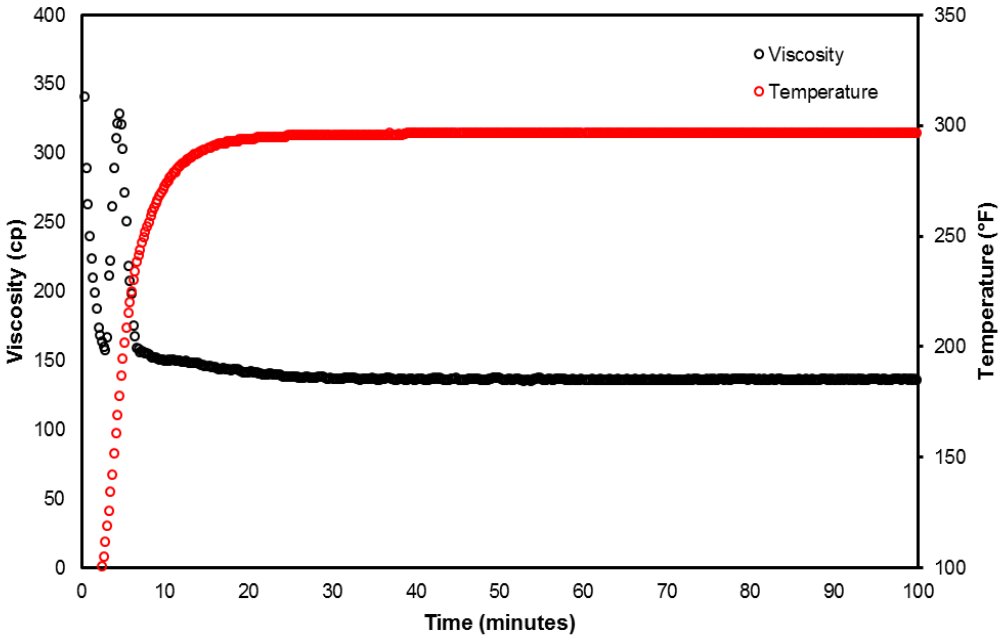

Figure 25. Stability and performance of VES 1- CNT (0.2 wt%) solution at 300 °F

Figure 26 demonstrates the results of viscosity measurements for the systems contained VES 2 in the presence and absence of CNT. The main difference in the rheological behaviors of VES 1 and VES 2 was that VES 2 showed a single peak in its viscosity profile, while as it is shown in Figure 24, VES 1 had a viscosity profile with two peaks. This

dissimilarity can be attributed to the fact that VES 2 cannot form a micellar system consists of branched wormlike micelles, which may be related to its chemical structure. It can be seen from Figure 25 that upon addition of 0.02 and 0.2 wt% CNT to the VES 2 solution, the viscosity performance was enhanced significantly. Such a change was more notable at the viscosity peak as its reading value was increased 31 and 39 % after the addition of 0.02 and 0.2 wt% CNT, respectively. The increase in the viscosity profile of VES 2 can be attributed to the formation of longer wormlike micelles and further entanglement of these micelles and forming a transient network.

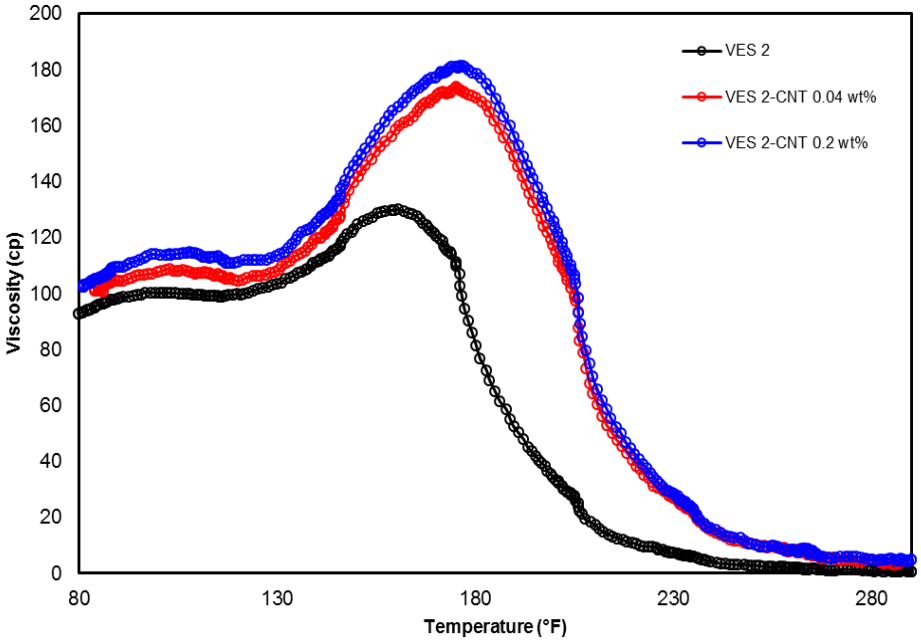

Figure 26. Viscosity profile of VES 2 in the presence of 0, 0.02, and 0.2 wt% CNT

Figure 27 shows the viscosity profile for the solution of VES 2 (6%) and CNT (0.2 wt%) over 100 minutes at 200 °F. It can be seen that the solution maintained its viscosity and

stayed stable for a reasonable period of time. The differences between VES 1 and VES 2 responses to the addition of CNT can be attributed to their interactions with CNT, which will be discussed later in this chapter.

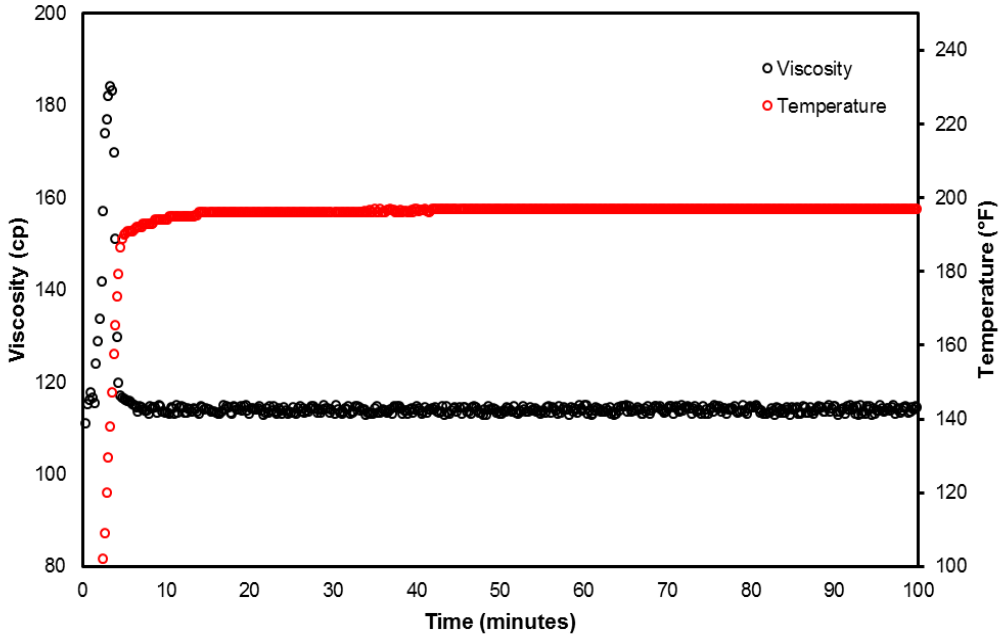

Figure 27. Stability and performance of VES 2- CNT (0.2 wt%) solution at 300 °F

Characterization of the Reactions/Interactions of CNT with VES Solutions

IR Spectroscopy Results

Figure 28 shows the IR spectrum of VES 1 with and without CNT. The broad peak at 3340 cm^{-1} can be assigned to OH/NH stretching vibration. The peaks below 3000 cm^{-1} are representative of CH stretching vibrations. The C=O stretching vibration can be detected through the peak at 1641 cm^{-1}. After the addition of 0.2 wt% CNT to VES 1 solution, the OH/NH representing peak shifted to 3345 cm^{-1}. Furthermore, the C=O stretching vibration

peak shifted to 1635 cm^{-1} upon the addition of CNT. The shifting can be explained by newly formed hydrogen bonding between the terminal functional groups of the CNT and the C=O. It should be noted that there is no shift in the CH stretching vibrations of VES, which means the CNT interacts with the hydrophilic head group rather the hydrophobic tail.

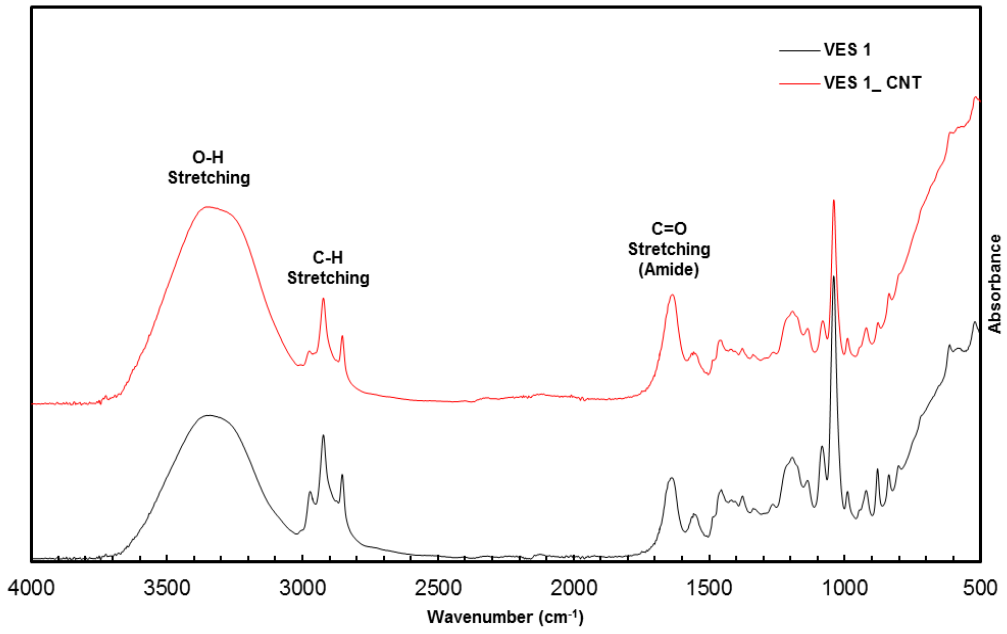

Figure 28. IR spectrums of VES 1 with and without CNT

The observed shifts in the IR spectrum of VES 1 upon the addition of CNT can be further explained by the resonance structure of the amide group within the surfactant compound. Amide can have two resonance structures, as indicated in Figure 29. Depending on the media, one resonance scheme is more optimal than the other. When there is an influx of protons within the media, the right side structure is more optimal. Therefore, upon the addition of the CNT, the right resonance structure is more optimal and explains the different

frequency shifts. C=O becomes C-O^- which the third lone pair can hydrogen bond and go to a lower energy state. The NH becomes NH^+, which, when hydrogen bonding occurs, would cause the N-H bond to shrink and go into a higher energy state.

Figure 29. Resonance structures of the amide functional group

For VES 2, the IR spectrum (Figure 30) showed shifting in the C=O and NH region to a lower frequency. Such behavior may be explained by resonance structures of the amide functional group. Within the VES 2 structure, there is an N-oxide group neighbored to the amide that can work as a withdrawing group. Hence, the signal assigned to C=O would appear at different frequencies. As a result, C=O became a probe of finding newly formed interactions like hydrogen bonding, as there was significant shifting in this region in both VES solutions. The IR data of the present study supports the Qin, et al. 2017 study on zwitterionic surfactants and CNT [1]. Shifting of the OH/NH stretch bands upon the addition of CNT indicating the interactions between the hydroxyl group of the CNT and the NH group of the surfactant. Also, the data indicates that there are significant shifts in the C=O group, further supporting the claim. Table 3 summarizes the IR peak assignments for each of the VES samples before and after the addition of CNT.

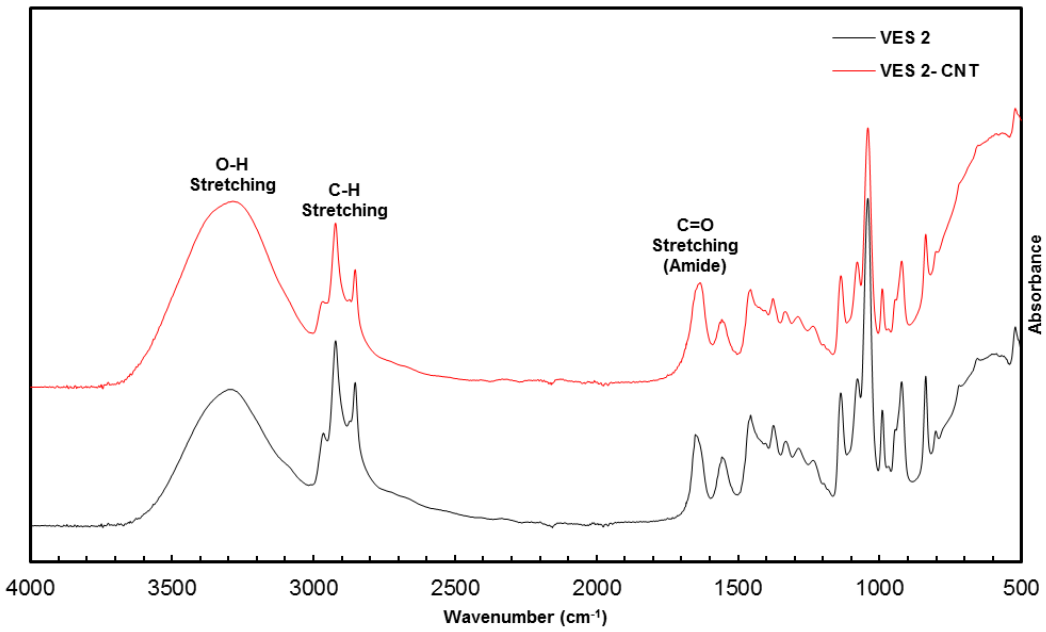

Figure 30. IR spectrums of VES 2 with and without CNT

NMR Spectroscopy Results

To further investigate the intermolecular interactions between the VES and CNT, ^{1}H NMR spectroscopy has been employed. ^{1}H NMR analysis can be used to find whether additives, such as nanomaterials, can have any interaction or reaction with the VES molecules. The addition of multiwalled functionalized CNT into a neutral, water-based environment may lead to a downfield or upfield shift in ^{1}H NMR signals due to the change of the microenvironment of the protons [85–87]. On the other hand, chemical shifting is sensitive to the chemical nature of the related protons and penetration of protons into nonpolar or polar media that may induce an upfield or downfield shift due to the change in magnetic susceptibility of the protons [85,88]. The amount of shifting, if present, in proton signals, depends on various conditions, including temperature and concentration. Since these

experiments manipulated temperature and concentration, the amount of shifting of the VES solutions varied from one VES to another one.

Table 3. Assigned functional groups in IR spectrums of VES samples with and without CNT

Assigned functional group	No CNT	0.02 wt% CNT	Shift amount
VES 1			
OH-/NH- Stretch	3340	3345	5
CH- Stretch	2923	2923	0
C=O Stretch	1641	1635	-6
VES 2			
OH-/NH- Stretch	3296	3284	-12
CH- Stretch	2922	2922	0
C=O Stretch	1651	1633	-18

Figure 31 depicts the ^{1}H NMR of VES 1 in D_2O; however, the representative peaks of VES cannot be fully detected in this spectrum. This problem may arise from the relatively low concentration (~15%) of the surfactant within the VES solution and the effects of D_2O as NMR solvent that usually causes signal broadening. To avoid signal broadening effects of D_2O, the solutions for ^{1}H NMR study were prepared in DMSO-d6. For resembling rheology test conditions, 6% VES solution was used, and such a concentration was not enough for the full detection of all VES signals.

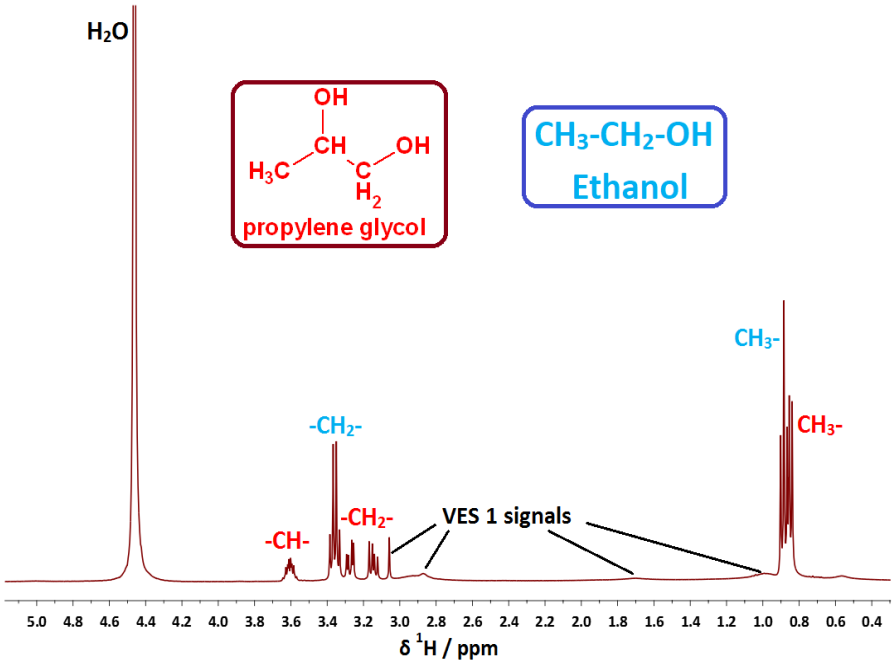

Figure 31. ^{1}H NMR of VES 1 in D_2O at 78°F

Figure 32 shows the ^{1}H NMR spectrum of VES 1 in DMSO-d6. As can be seen from this figure, signals of the solvents (methanol, ethanol, propylene glycol) and the surfactant tail are the dominant signals in the spectrum. A singlet signal at 3.36 ppm represents a significant amount of water content. A set of signals at 1.05 (triplet), 3.44 (multiplet), and 4.37 ppm (triplet) with a ratio of 3:2:1 can be related to CH_3 group, CH_2 group, and OH group of ethanol, respectively. A doublet at 0.99 ppm related to CH_3 group, two sets of doublet of doublet at 3.16, and 3.24 ppm can be assigned to the asymmetric CH_2 group, and a sextet at 3.55 ppm can be attributed to the CH group. A doublet at 4.42 ppm and a triplet at 4.48 ppm indicate the two hydroxide (OH) groups of 1,2-propanediol (propylene glycol). These assignments are in good agreement with report chemical shifts in the literature (Fulmer et al. 2010). The rest of the signals for this mixture are indicative of the active surfactant in the solution. To eliminate

the signals associated with solvents in the spectrum, the stock solution was substituted with the model compound head group of the surfactant called SMA.

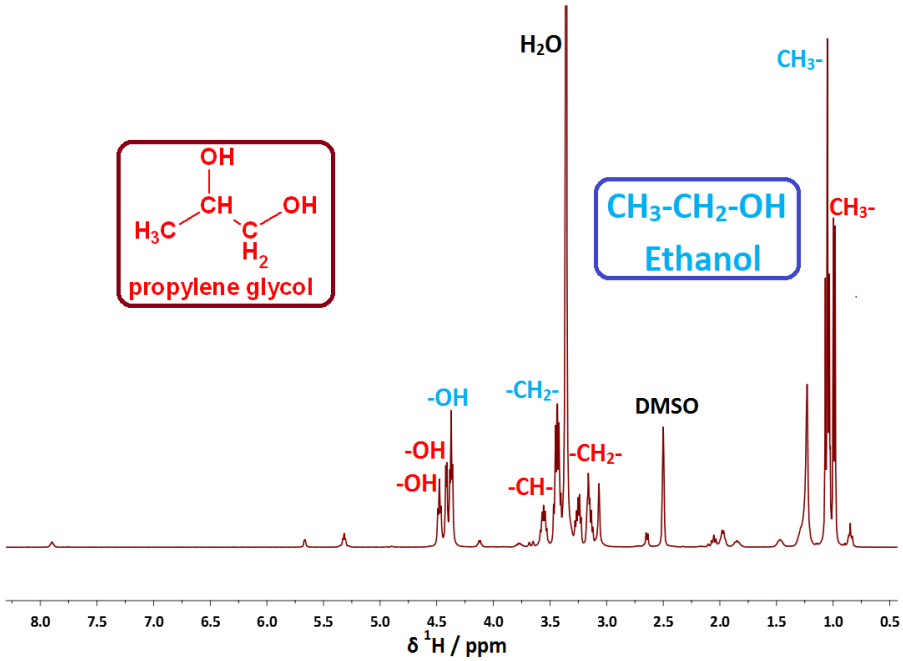

Figure 32. ^{1}H NMR of VES 1 in DMSO-d6 at 78°F

Figure 33 shows the ^{1}H NMR spectrum of VES 2 at ambient conditions. These results demonstrate that VES 2 contains propylene glycol as a solvent and a nonionic surfactant as an active agent. A singlet signal at 3.35 ppm represents water content, which is in the expected region because water position, in general, hydroxide signal, depends on solvent, other substrates, and temperature. A set of signals with 3:1:1:1:2 ratio correlate with each other. A doublet at 0.99 ppm, two sets of doublet of doublet at 3.16 and 3.24 ppm, a sextet signal at 3.55 ppm, and a broad signal at 4.48 ppm with 3:1:1:1:2 ratio can be assigned to CH_3 group,

asymmetric CH_2 group, CH group, and two hydroxide (OH) groups of propylene glycol respectively. The rest of the signals for this mixture are related to the nonionic surfactant.

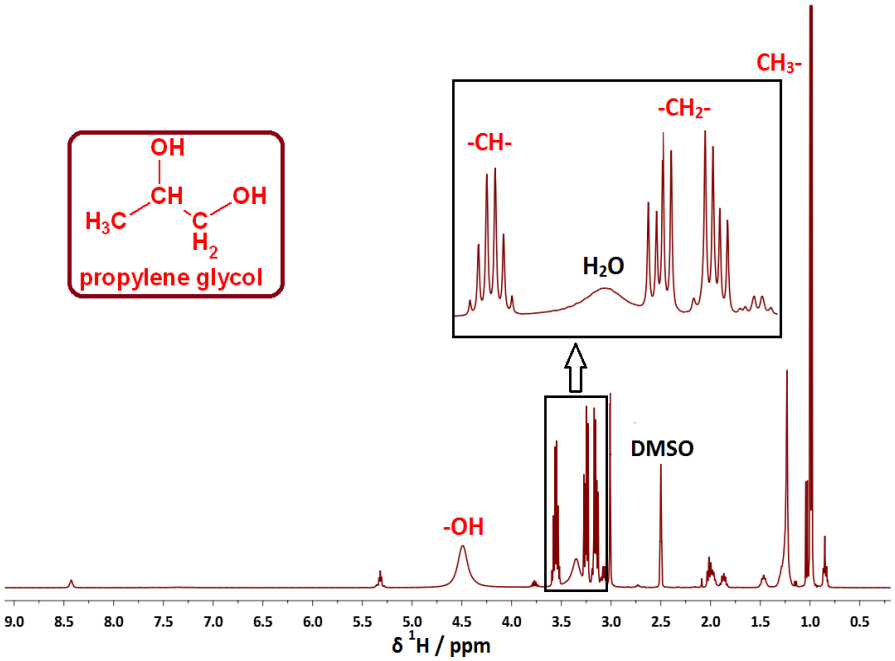

Figure 33. ^{1}H NMR of VES 2 in DMSO-d6 at 78°F. The box shows the selected region in the larger scale

Figure 34 shows the ^{1}H NMR spectrum of the SMA in D_2O. Two singlets at 5.74 and 5.50 ppm can be assigned to two protons with 1:1 ratio belong to the olefin part of SMA (H1 and H2). However, the differentiation of these peaks cannot be done by just using the 1D NMR spectroscopy technique. A multiplet at 3.51 ppm belongs to the CH_2 group neighboring to the amide group, H4. Because of using D_2O as a solvent and fast deuterium hydrogen exchange between acidic protons such as hydrogen of the NH group, this signal cannot be observed, but H/D coupling is visible in H4. Due to the similarity of their chemical

environments (two CH_2 groups on both sides of the NMe_2 group), H8 and H6 show two triplets with $^3J_{HH}$ = 5.6 Hz having close chemical shifts at 3.40 and 3.38 ppm that somehow overlapped. A singlet at 3.14 ppm with the integration of 6 is related to the NMe_2 group. A triplet at 3.00 ppm with $^3J_{HH}$ = 7.1 Hz is representative of the CH_2 group, H10. Two similar multiplets at 2.23 and 2.07 ppm belong to two CH_2 groups, H9 and H5. A singlet at 1.96 ppm belongs to the CH_3 group, H3.

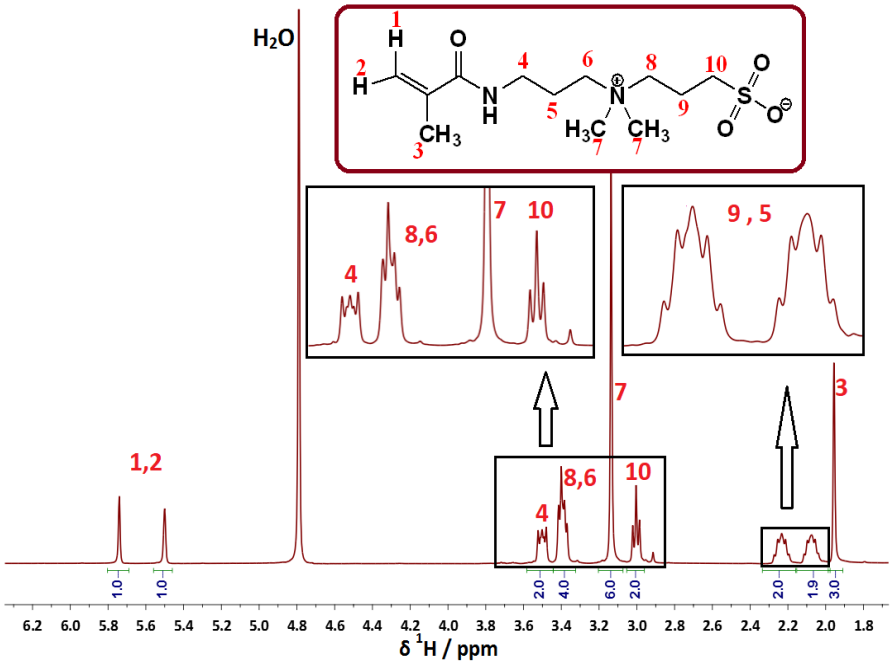

Figure 34. ^{1}H NMR of SMA in D_2O at 78°F. Boxes show the selected regions in the larger scale

Figure 35 shows the ^{1}H NMR spectrums of SMA in the presence and absence of CNT. An upfield shift ($\Delta\delta < 0$) in the peaks of all protons can be detected upon the addition of CNT. Although the peak heights are changed for the terminal methyl protons (H3) located farthest

from the head, their locations are barely altered. Such an observation may indicate that once CNT inserted into the micelle network in VES 1 or VES 2, it would not interact significantly with the tail or the hydrophilic region of the surfactants. Instead, new interactions may form between the polar portion of the surfactants and the hydroxyl/ carboxyl terminal groups of CNT.

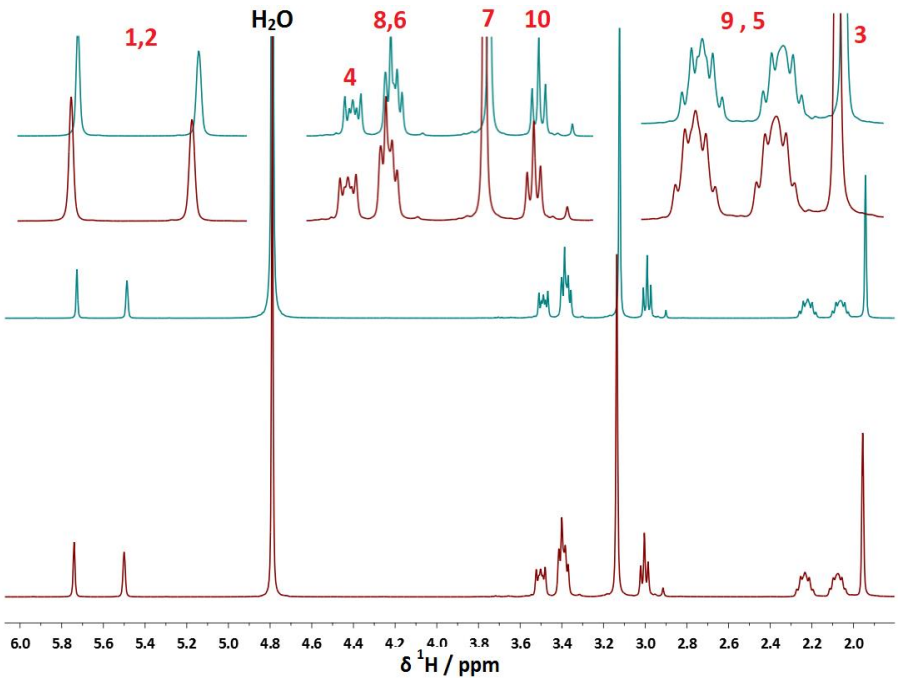

Figure 35. ^{1}H NMR of (bottom) SMA in D_2O at 78°F, (top) SMA + CNT in D_2O at 78° F. Some regions are expanded to show the shifts

Figure 36 shows the NMR spectrums of VES 2 before and after adding CNT at both room temperature and 200 °F. Although the spectrum still shows the signals of the solvents, the higher surfactant concentration (~50%) in the VES 2 solution allowed for obtaining broad yet distinct signals in the NMR spectrum. Upon the addition of CNT, the peak at 3.2 ppm

becomes broader and shifted upfield slightly. After heating the solution, this shift becomes even broader due to the strong hydrogen bonding between CNT and VES molecules. In other words, upon heating, the orientation of the surfactant compound may change, resulting in some protons being able to interact with the CNT.

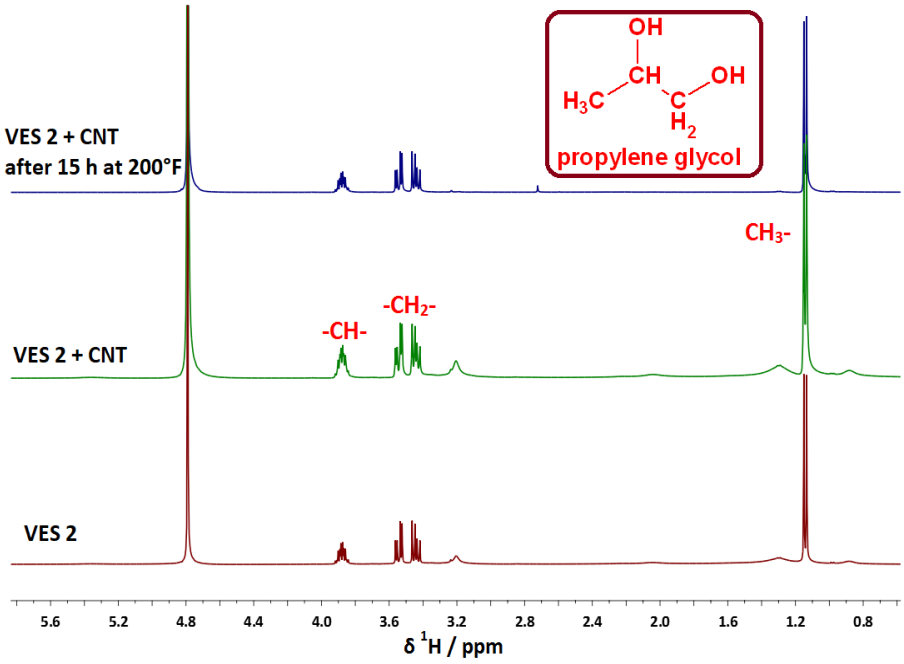

Figure 36. ^{1}H NMR of (bottom) VES 2 solution (6%) in D2O at 78°F, (middle) mixture of VES 2 solution (6%) + CNT (0.04%) in D2O at 78°F, and (top) VES 2 solution (6%) + CNT (0.04%) in D2O after 15h at 200°F

CHAPTER VI

CONCLUSIONS

VES Interactions with Fe (III) at Acidic Conditions

Formation of wormlike micelles in a system containing a zwitterionic C_{22}-tailed sulfobetaine surfactant in the presence of Fe^{3+} in HCl is shown by rheological and SAXS techniques. The transition from viscoelastic behavior to that of a non-Maxwellian elastic gel-like behavior after the addition of Fe^{3+} is confirmed through dynamic viscoelastic measurements. The presence of wormlike micelles in the solutions is affirmed by evaluating the SAXS profiles of samples. Rheological and visual experimental results indicate the sensitivity of EDAS to tested inorganic salt ($FeCl_3$). The nature of such a transition in the physical behavior of the surfactant after the addition of Fe^{3+} was characterized and studied by IR, single crystal X-ray, and UV-visible spectroscopy techniques. The noncovalent interaction of EDAS amide functional group is shown by IR spectroscopy (gradual shifting in the C=O of amide). The presence of *trans*-$[FeCl_2(H_2O)_4]Cl$ structure in the solid state was revealed for the first time using the single crystal X-ray technique. The existence of this structure in the solution state is confirmed by UV-visible data, which is also in good agreement with the previously proposed structure. The strong hydrogen bonding between non-coordinated Cl^- and hydrogen of coordinated water was detected in the reported crystal structure. Such hydrogen bonding results in screening the repulsion forces between surfactants headgroups (which is also confirmed by the reduction of A_{min} value after addition of Fe^{3+}) and, consequently, the formation of longer wormlike micelles. The generation of such a network leads to the

alteration of solution behavior from a viscoelastic solution to a gel-like elastic material with high viscosity.

Interactions/ Reactions of Corrosion Inhibitors with VES-Based Systems

The generation of acidic conditions after mixing VES and corrosion inhibitors can be extremely detrimental to the rheological performance of amide containing a VES-based system. This work identified VES decomposition is the primary mechanism that impairs viscosity. The generation of such an environment prevents viscosity build-up and any temperatures or aging stages. VES solutions do not alter the performance of corrosion inhibitors significantly; however, in some cases, strong interactions between VES and corrosion inhibitors would increase corrosion rates in a low-carbon-steel environment.

The presence of weak acid in the corrosion-inhibitor composition may enhance the viscosity performance of amine-based VES in a certain temperature range through acid-base reactions. These types of reactions would facilitate the formation of wormlike micelles and consequently causes higher viscosity in the solutions. Weak interactions between corrosion-inhibitor solvents such as methanol and VES amide group can slightly affect the rheological performances of VES-based systems. The overall rheological behavior would remain the same; however, a small drop in viscosity reading may be observed.

Interactions/ Reactions of Multifunctionalized CNT with VES-Based Fracturing Fluids

A new type of nano VES-based fracturing fluid with high thermal stability and promising rheological behavior is introduced and investigated in the present study. The

addition of CNT to a nonionic VES solution leads to achieving higher viscosity at the entire tested temperature range. The addition of CNT to a zwitterionic VES leads to higher stability in terms of viscosity at high temperature (300 °F) conditions.

The interaction of CNT with VES solutions is characterized to be mainly hydrogen bonding between functional groups of CNT and amide and N-oxide groups of tested VES solutions. These interactions result in the screening of repulsion forces between surfactant headgroups so that longer wormlike micelles can be formed in the solution. Since the VES-CNT mixture is a dynamic system, there is no need for any breaker, and the VES and CNT interactions would be disrupted by matrix alteration (such as hydrocarbon production).

REFERENCES

[1] Qin W, Yue L, Liang G, Jiang G, Yang J, Liu Y. Effect of multi-walled carbon nanotubes on linear viscoelastic behavior and microstructure of zwitterionic wormlike micelle at high temperature. Chem Eng Res Des 2017;123:14–22. https://doi.org/10.1016/j.cherd.2017.04.027.

[2] Zou W, Tan G, Jiang H, Vogtt K, Weaver M, Koenig P, et al. From well-entangled to partially-entangled wormlike micelles. Soft Matter 2019;15:642–55. https://doi.org/10.1039/C8SM02223B.

[3] Magid LJ. The surfactant-polyelectrolyte analogy. J Phys Chem B 1998;102:4064–74. https://doi.org/10.1021/jp9730961.

[4] Rehage H, Hoffmann H. Viscoelastic surfactant solutions:Model systems for theological research. Mol Phys 1991;74:933–73. https://doi.org/10.1080/00268979100102721.

[5] Oelschlaeger C, Willenbacher N. Rheological properties of aqueous solutions of cetylpyridinium chloride in the presence of sodium chlorate. Rheol Acta 2011;50:655–https://doi.org/10.1007/s00397-011-0548-z.

[6] Kalur GC, Frounfelker BD, Cipriano BH, Norman AI, Raghavan SR. Viscosity increase with temperature in cationic surfactant solutions due to the growth of wormlike micelles. Langmuir 2005;21:10998–1004. https://doi.org/10.1021/la052069w.

[7] Barhoum S, Castillo R, Yethiraj A. Characterization of dynamics and internal structure

of a mixed-surfactant wormlike micellar system using NMR and rheometry. Soft Matter 2012;8:6950–7. https://doi.org/10.1039/c2sm25237f.

[8] Raghavan SR, Edlund H, Kaler EW. Cloud-point phenomena in wormlike micellar systems containing cationic surfactant and salt. Langmuir 2002;18:1056–64. https://doi.org/10.1021/la011148e.

[9] Bewersdorff HW, Ohlendorf D. The behaviour of drag-reducing cationic surfactant solutions. Colloid Polym Sci 1988;266:941–53. https:// doi.org/10.1007/BF01410851.

[10] Ohlendorf D, Interthal W, Hoffman H. Surfactant systems for drag reduction: physico-chemical properties and rheological behaviour. Rheol Acta 1986;25:468–86. https://doi.org/10.1007/BF01774397.

[11] Lungwitz BR, Fredd CN, Brady ME, Miller MJ, Ali SA, Hughes KN. Diversion and Cleanup Studies of Viscoelastic Surfactant-Based Self-Diverting Acid. SPE Prod Oper 2007;22:121–7. https://doi.org/10.2118/86504-PA.

[12] Al-Muntasheri GA. A critical review of hydraulic-fracturing fluids for moderate- to ultralow- permeability formations over the last decade. SPE Prod Oper 2014;29:243–https://doi.org/10.2118/169552-PA.

[13] Hull Katherine L, Mohammed S, Al-Muntasheri Ghaithan A. Recent advances in viscoelastic surfactants for improved production from hydrocarbon reservoirs. SPE J., vol. 21, Society of Petroleum Engineers; 2016, p. 1340–57. https://doi.org/10.2118/173776-pa.

[14] Nasr-El-Din HA, Chesson JB, Cawiezel KE, Devine CS. Lessons learned and guidelines for matrix acidizing with viscoelastic surfactant diversion in carbonate

formations. Proc - SPE Annu Tech Conf Exhib 2006;3.

[15] Daniel S, Morris L, Chen Y, Brady ME, Lungwitz BR, George L, et al. New Visco-Elastic Surfactant Formulations Extend Simultaneous Gravel-Packing and Cake-Cleanup Technique to Higher-Pressure and Higher-Temperature Horizontal Open-Hole Completions: Laboratory Development and a Field Case History From the North Sea. Int. Symp. Exhib. Form. Damage Control, 2002. https://doi.org/10.2118/73770-MS.

[16] Nasr-El-Din HA, Taylor KC, Al-Hajji HH. Propagation of Cross-linkers Used in In-Situ Gelled Acids in Carbonate Reservoirs. Proc. - SPE Symp. Improv. Oil Recover., Society of Petroleum Engineers; 2002, p. 1152–71. https:// doi.org/10.2523/75257-ms.

[17] Feng Y, Chu Z, Dreiss CA. Smart Wormlike Micelles: Design, Characteristics and Applications. 2015. https://doi.org/10.1007/978-3-662-45950-8.

[18] Shrestha RG, Abezgauz L, Danino D, Sakai K, Sakai H, Abe M. Structure and dynamics of poly(oxyethylene) cholesteryl ether wormlike micelles: Rheometry, SAXS, and cryo-TEM studies. Langmuir 2011;27:12877–83. https://doi.org/10.1021/la202879f.

[19] Sharma SC, Rodríguez-Abreu C, Shrestha LK, Aramaki K. Short haired wormlike micelles in mixed nonionic fluorocarbon surfactants. J Colloid Interface Sci 2007;314:223–9. https://doi.org/10.1016/j.jcis.2007.05.066.

[20] Kumars R, Kalur GC, Ziserman L, Danino D, Raghavan SR. Wormlike micelles of a C22-tailed zwitterionic betaine surfactant: From viscoelastic solutions to elastic gels. Langmuir 2007;23:12849–56. https://doi.org/10.1021/la7028559.

[21] Feng Y, Chu Z. pH-Tunable wormlike micelles based on an ultra-long-chain "pseudo" gemini surfactant. Soft Matter 2015;11:4614–20. https://doi.org/10.1039/C5SM00677E.

[22] Silva KN, Novoa-Carballal R, Drechsler M, Müller AHE, Penott-Chang EK, Müller AJ. The influence of concentration and pH on the structure and rheology of cationic surfactant/hydrotrope structured fluids. Colloids Surfaces A Physicochem Eng Asp 2016;489:311–21. https://doi.org/10.1016/j.colsurfa.2015.10.054.

[23] Dreiss CA, Feng Y. Wormlike micelles : advances in systems, characterisation and applications. 2017.

[24] Bergström LM, Tehrani-Bagha A, Nagy G. Growth behavior, geometrical shape, and second CMC of micelles formed by cationic gemini esterquat surfactants. Langmuir 2015;31:4644–53. https://doi.org/10.1021/acs.langmuir.5b00742.

[25] Israelachvili JN, Mitchell DJ, Ninham BW. Theory of self-assembly of hydrocarbon amphiphiles into micelles and bilayers. J Chem Soc Faraday Trans 2 Mol Chem Phys 1976;72:1525–68. https://doi.org/10.1039/F29767201525.

[26] Rehage H, Hoffmann H. Rheological properties of viscoelastic surfactant systems. J Phys Chem 1988;92:4712–9. https://doi.org/10.1021/j100327a031.

[27] Shikata T, Hirata H, Kotaka T. Micelle Formation of Detergent Molecules in Aqueous Media. 3. Viscoelastic Properties of Aqueous Cetyltrimethylammonium Bromide-Salicylic Acid Solutions. Langmuir 1989;5:398–405. https://doi.org/10.1021/la00086a020.

[28] Cates ME, Candau SJ. Statics and dynamics of worm-like surfactant micelles. J Phys

Condens Matter 1990;2:6869–92. https://doi.org/10.1088/0953-8984/2/33/001.

[29] Kern F, Zana R, Candau SJ. Rheological Properties of Semidilute and Concentrated Aqueous Solutions of Cetyltrimethylammonium Chloride in the Presence of Sodium Salicylate and Sodium Chloride. Langmuir 1991;7:1344–51. https://doi.org/10.1021/la00055a010.

[30] Khatory A, Lequeux F, Kern F, Candau SJ. Linear and Nonlinear Viscoelasticity of Semidilute Solutions of Wormlike Micelles at High Salt Content. Langmuir 1993;9:1456–64. https://doi.org/10.1021/la00030a005.

[31] Song B, Hu Y, Song Y, Zhao J. Alkyl chain length-dependent viscoelastic properties in aqueous wormlike micellar solutions of anionic gemini surfactants with an azobenzene spacer. J Colloid Interface Sci 2010;341:94–100. https://doi.org/10.1016/j.jcis.2009.09.023.

[32] Chu Z, Feng Y. Amidosulfobetaine surfactant gels with shear banding transitions. Soft Matter 2010;6:6065–7. https://doi.org/10.1039/c0sm00874e.

[33] Han Y, Feng Y, Sun H, Li Z, Han Y, Wang H. Wormlike micelles formed by sodium erucate in the presence of a tetraalkylammonium hydrotrope. J Phys Chem B 2011;115:6893–902. https://doi.org/10.1021/jp2004634.

[34] Han Y, Chu Z, Sun H, Li Z, Feng Y. “Green” anionic wormlike micelles induced by choline. RSC Adv 2012;2:3396–402. https://doi.org/10.1039/c2ra20136d.

[35] Granek R, Cates ME. Stress relaxation in living polymers: Results from a Poisson renewal model. J Chem Phys 1992;96:4758–67. https://doi.org/10.1063/1.462787.

[36] Hassan PA, Valaulikar BS, Manohar C, Kern F, Bourdieu L, Candau SJ. Vesicle to

Micelle Transition: Rheological Investigations. Langmuir 1996;12:4350–7. https://doi.org/10.1021/la960269p.

[37] Davies TS, Ketner AM, Raghavan SR. Self-assembly of surfactant vesicles that transform into viscoelastic wormlike micelles upon heating. J Am Chem Soc 2006;128:6669–75. https://doi.org/10.1021/ja060021e.

[38] Lin Y, Han X, Cheng X, Huang J, Liang D, Yu C. pH-regulated molecular self-assemblies in a cationic-anionic surfactant system: From a “1-2” surfactant pair to a “1-1” surfactant pair. Langmuir 2008;24:13918–24. https://doi.org/10.1021/la802593n.

[39] Johnsson M, Wagenaar A, Stuart MCA, Engberts JBFN. Sugar-based gemini surfactants with pH-dependent aggregation behavior: Vesicle-to-micelle transition, critical micelle concentration, and vesicle surface charge reversal. Langmuir 2003;19:4609–18. https://doi.org/10.1021/la0343270.

[40] Johnsson M, Wagenaar A, Engberts JBFN. Sugar-based gemini surfactant with a vesicle-to-micelle transition at acidic pH and a reversible vesicle flocculation near neutral pH. J Am Chem Soc 2003;125:757–60. https://doi.org/10.1021/ja028195t.

[41] Ghosh S, Khatua D, Dey J. Interaction between zwitterionic and anionic surfactants: Spontaneous formation of zwitanionic vesicles. Langmuir 2011;27:5184–92. https://doi.org/10.1021/la1040147.

[42] Wu H, Zhou Q, Xu D, Sun R, Zhang P, Bai B, et al. SiO2 nanoparticle-assisted low-concentration viscoelastic cationic surfactant fracturing fluid. J Mol Liq 2018;266:864–9. https://doi.org/10.1016/j.molliq.2018.06.107.

[43] Li L, Nasr-El-Din HA, Crews JB, Hughes B, Cawiezel KE. Impact of organic acids/chelating agents on the rheological properties of an amidoamine-oxide surfactant. SPE Prod Oper 2011;26:30–40. https://doi.org/10.2118/128091-pa.

[44] Yang J. Viscoelastic wormlike micelles and their applications. Curr Opin Colloid Interface Sci 2002;7:276–81. https://doi.org/10.1016/S1359-0294(02)00071-7.

[45] Fontana C, Muruaga E, Perez DR, Cavazzoli GD, Krenz A. Successful application of a high temperature viscoelastic surfactant (VES) fracturing fluids under extreme conditions in patagonian wells, San Jorge Basin. 69th Eur. Assoc. Geosci. Eng. Conf. Exhib. 2007 Secur. Futur. Inc. SPE Eur. 2007, vol. 4, Society of Petroleum Engineers; 2007, p. 2231–45. https://doi.org/10.2118/107277-ms.

[46] Pötschke P, Fornes TD, Paul DR. Rheological behavior of multiwalled carbon nanotube/polycarbonate composites. Polymer (Guildf) 2002;43:3247–55. https://doi.org/10.1016/S0032-3861(02)00151-9.

[47] Afra S, Samouei H, Mahmoudkhani R, Nasr-El-Din H. A novel nanotube/Ves-based high temperature high pressure fracturing fluid. Proc. - SPE Int. Symp. Form. Damage Control, vol. 2020–Febru, Society of Petroleum Engineers; 2020, p. 19–21. https://doi.org/10.2118/199231-MS.

[48] Gougler PD, Hendrick JE, Coulter AW. Field investigation identifies source and magnitude of iron problems. Soc. Pet. Eng. - SPE Prod. Oper. Symp. POS 1985, 1985. https://doi.org/10.2523/13812-ms.

[49] Afra S, Samouei H, Nasr-El-Din HA. Characterization of iron interaction with viscoelastic surfactant VES-based Acidizing fluid. SPE West. Reg. Meet., vol. 2019–

April, 2019. https://doi.org/10.2118/194862-ms.

[50] Afra S, Samouei H, Truong P, Nasr-El-Din H. Micellar growth and network formation in acidic solutions of a sulfobetaine zwitterionic surfactant triggered by an inorganic salt. Soft Matter 2020;16:4494–501. https://doi.org/10.1039/d0sm00399a.

[51] Taylor K, Nasr-El-Din H, Al-Alawi M. Systematic Study of Iron Control Chemicals Used During Well Stimulation. SPE J 1999;4:19–24. https://doi.org/10.2118/54602-PA.

[52] Walker ML, Dill WR, Besler MR, Mcfatridge DG, Services H. Iron Control in West Texas Sour-Gas Wells Provides Sustained Production Increases. SPE J 1991:603–7. https://doi.org/10.2118/20122-PA.

[53] Afra S, Samouei H, Nasr-El-Din HA. Characterization of iron interaction with viscoelastic surfactant VES-based stimulation fluid. SPE Middle East Oil Gas Show Conf. MEOS, Proc., vol. 2019–March, 2019. https://doi.org/10.2118/194862-ms.

[54] Finšgar M, Jackson J. Application of corrosion inhibitors for steels in acidic media for the oil and gas industry: A review. Corros Sci 2014;86:17–41. https://doi.org/10.1016/j.corsci.2014.04.044.

[55] Ng JH, Almubarak T, Nasr-El-Din HA. Low-carbon-steel corrosion at high temperatures by aminopolycarboxylic acids. SPE Prod. Oper., vol. 33, 2018, p. 131–https://doi.org/10.2118/188007-PA.

[56] Okafor PC, Liu X, Zheng YG. Corrosion inhibition of mild steel by ethylamino imidazoline derivative in CO2-saturated solution. Corros Sci 2009;51:761–8. https://doi.org/10.1016/j.corsci.2009.01.017.

[57] Zhang G, Chen C, Lu M, Chai C, Wu Y. Evaluation of inhibition efficiency of an imidazoline derivative in CO2-containing aqueous solution. Mater Chem Phys 2007;105:331–40. https://doi.org/10.1016/j.matchemphys.2007.04.076.

[58] Frenier WW, Growcock FB, Lopp VR. alpha -ALKENYLPHENONES-A NEW CLASS OF ACID CORROSION INHIBITORS. Corrosion 1988;44:590–8. https://doi.org/10.5006/1.3584970.

[59] Growcock FB. Corrosion kinetics of J55 steel in hydrochloric acid inhibited with benzoyl allyl alcohol. Corrosion 1989;45:393–401. https://doi.org/10.5006/1.3582034.

[60] Quraishi MA, Jamal D. Technical note: CAHMT - A new and eco-friendly acidizing corrosion inhibitor. Corrosion 2000;56:983–5. https:// doi.org/10.5006/1.3294388.

[61] Quraishi MA, Jamal D. Corrosion inhibition of N-80 steel and mild steel in 15% boiling hydrochloric acid by a triazole compound - SAHMT. Mater Chem Phys 2001;68:283–https://doi.org/10.1016/S0254-0584(00)00369-2.

[62] Baddini AL de Q, Cardoso SP, Hollauer E, Gomes JA da CP. Statistical analysis of a corrosion inhibitor family on three steel surfaces (duplex, super-13 and carbon) in hydrochloric acid solutions. Electrochim Acta 2007;53:434–46. https://doi.org/10.1016/j.electacta.2007.06.050.

[63] Dehri I, Özcan M. The effect of temperature on the corrosion of mild steel in acidic media in the presence of some sulphur-containing organic compounds. Mater Chem Phys 2006;98:316–23. https://doi.org/10.1016/j.matchemphys.2005.09.020.

[64] Gomaa AM, Cutler J, Qu Q, Cawiezel KE. Acid placement: An effective VES system to stimulate high-temperature carbonate formations. SPE Prod. Oper. Symp. Proc., vol.

2, Society of Petroleum Engineers (SPE); 2012, p. 1112–32. https://doi.org/10.2118/157316-ms.

[65] Afra S, Samouei H, Nasr-El-Din HA. NMR Investigation of Viscoelastic Surfactant Compatibility with Corrosion Inhibitors. SPE J 2020. https:// doi.org/10.2118/204214-pa.

[66] Afra S, Samouei H, Nasr-El-Din H. NMR investigation of viscoelastic surfactants compatibility with corrosion inhibitors. Int. Pet. Technol. Conf. 2020, IPTC 2020, International Petroleum Technology Conference (IPTC); 2020. https://doi.org/10.2523/iptc-19601-ms.

[67] Raghavan SR, Fritz G, Kaler EW. Wormlike micelles formed by synergistic self-assembly in mixtures of anionic and cationic surfactants. Langmuir 2002. https://doi.org/10.1021/la0115583.

[68] Nasr-El-Din HA, Chesson JB, Cawiezel KE, Devine CS. Lessons learned and guidelines for matrix acidizing with viscoelastic surfactant diversion in carbonate formations. Proc. - SPE Annu. Tech. Conf. Exhib., vol. 3, Society of Petroleum Engineers; 2006, p. 2003–13. https://doi.org/10.2523/102468-ms.

[69] Hanafy A, Nasr-El-Din H, Rabie A, Zhou J. Effect of corrosion–inhibitor chemistry on the viscosity and corrosion rate of VES-based acids. Proc. - SPE Int. Symp. Oilf. Chem., vol. 2019, 2019.

[70] Yu M, Mu Y, Wang G, Nasr-Ei-din HA. Impact of hydrolysis at high temperatures on the apparent viscosity of carboxybetaine viscoelastic surfactant-based acid: Experimental and molecular dynamics simulation studies. SPE J., vol. 17, 2012, p.

1119–30. https://doi.org/10.2118/142264-PA.

[71] Chu Z, Feng Y, Su X, Han Y. Wormlike micelles and solution properties of a C22-tailed amidosulfobetaine surfactant. Langmuir 2010;26:7783–91. https://doi.org/10.1021/la904582w.

[72] Qiao Y, Lin Y, Wang Y, Li Z, Huang J. Metal-Driven Viscoelastic Wormlike Micelle in Anionic/Zwitterionic Surfactant Systems and Template-Directed Synthesis of Dendritic Silver Nanostructures. Langmuir 2011;27:1718–23. https://doi.org/10.1021/la104447d.

[73] Rulkens R, Wegner G, Thurn-Albrecht T. Cylindrical micelles of wormlike polyelectrolytes. Langmuir 1999;15:4022–5. https://doi.org/10.1021/la9809832.

[74] Varade D, Ushiyama K, Shrestha LK, Aramaki K. Wormlike micelles in Tween-80/CmEO3 mixed nonionic surfactant systems in aqueous media. J Colloid Interface Sci 2007;312:489–97. https://doi.org/10.1016/j.jcis.2007.02.090.

[75] Shrestha LK, Sharma SC, Sato T, Glatter O, Aramaki K. Small-angle X-ray scattering (SAXS) study on nonionic fluorinated micelles in aqueous system. J Colloid Interface Sci 2007;316:815–24. https://doi.org/10.1016/j.jcis.2007.08.005.

[76] Liu W, Etschmann B, Brugger J, Spiccia L, Foran G, McInnes B. UV-Vis spectrophotometric and XAFS studies of ferric chloride complexes in hyper-saline LiCl solutions at 25-90 °C. Chem Geol 2006;231:326–49. https://doi.org/10.1016/j.chemgeo.2006.02.005.

[77] Friedman HL. The Visible and Ultraviolet Absorption Spectrum of the Tetrachloroferrate(III) Ion in Various Media. J Am Chem Soc 1952;74:5–10.

https://doi.org/10.1021/ja01121a002.

[78] Gamlen GA, Jordan DO. A spectrophotometric study of the iron(III) chloro-complexes. J Chem Soc 1953:1435. https://doi.org/10.1039/jr9530001435.

[79] Cecchi L, De Sarlo F, Machetti F. 1,4-Diazabicyclo[2.2.2]octane (DABCO) as an efficient reagent for the synthesis of isoxazole derivatives from primary nitro compounds and dipolarophiles: The role of the base. European J Org Chem 2006:4852–https://doi.org/10.1002/ejoc.200600475.

[80] Srivastava TN, Saxena KL. Coordination compounds of ethylenediamine with diaryltin dihalides. J Inorg Nucl Chem 1971;33:3996–9. https:// doi.org/10.1016/0022-1902(71)80320-2.

[81] Pulla Rao C, Muralikrishna Rao A, Rao CNR. Crystal and Molecular Structures of Alkali- and Alkaline-Earth-Metal Complexes of N, N-Dimethylformamide. Inorg Chem 1984;23:2080–5. https://doi.org/10.1021/ic00182a020.

[82] Raghavan SR, Cipriano BH. Gel formation: Phase diagrams using tabletop rheology and calorimetry. Mol. Gels Mater. with Self-Assembled Fibrillar Networks, Springer Netherlands; 2006, p. 241–52. https://doi.org/10.1007/1-4020-3689-2_9.

[83] Oelschlaeger C, Schopferer M, Scheffold F, Willenbacher N. Linear-to-branched micelles transition: A rheometry and diffusing wave spectroscopy(DWS) study. Langmuir 2009;25:716–23. https://doi.org/10.1021/la802323x.

[84] Fulmer GR, Miller AJM, Sherden NH, Gottlieb HE, Nudelman A, Stoltz BM, et al. NMR chemical shifts of trace impurities: Common laboratory solvents, organics, and gases in deuterated solvents relevant to the organometallic chemist. Organometallics

2010;29:2176–9. https://doi.org/10.1021/om100106e.

[85] Kim BJ, Im SS, Oh SG. Investigation on the solubilization locus of aniline-HCl salt in SDS micelles with 1H NMR spectroscopy. Langmuir 2001;17:565–6. https://doi.org/10.1021/la0012889.

[86] Momot KI, Kuchel PW, Chapman BE, Deo P, Whittaker D. NMR study of the association of propofol with nonionic surfactants. Langmuir 2003;19:2088–95. https://doi.org/10.1021/la026722g.

[87] Vekariya RL, Aswal VK, Hassan PA, Soni SS. Influence of N -alkylpyridinium halide based ionic liquids on micellization of P123 in aqueous solutions: A SANS, DLS, and NMR study. Langmuir 2014;30:14406–15. https:// doi.org/10.1021/la502902n.

[88] Su YL, Liu HZ, Wang J, Chen JY. Study of salt effects on the micellization of PEO-PPO-PEO block copolymer in aqueous solution by FTIR spectroscopy. Langmuir 2002;18:865–71. https://doi.org/10.1021/la0106687.